PRESSURE DROP WITH SURFACE BOILING IN SMALL-DIAMETER TUBES

Thomas Dormer, Jr.
Arthur E. Bergles

September 1, 1964

Report No. 8767-31
Contract AF 19(604)-7344

Department of
Mechanical Engineering
Massachusetts Institute
of Technology

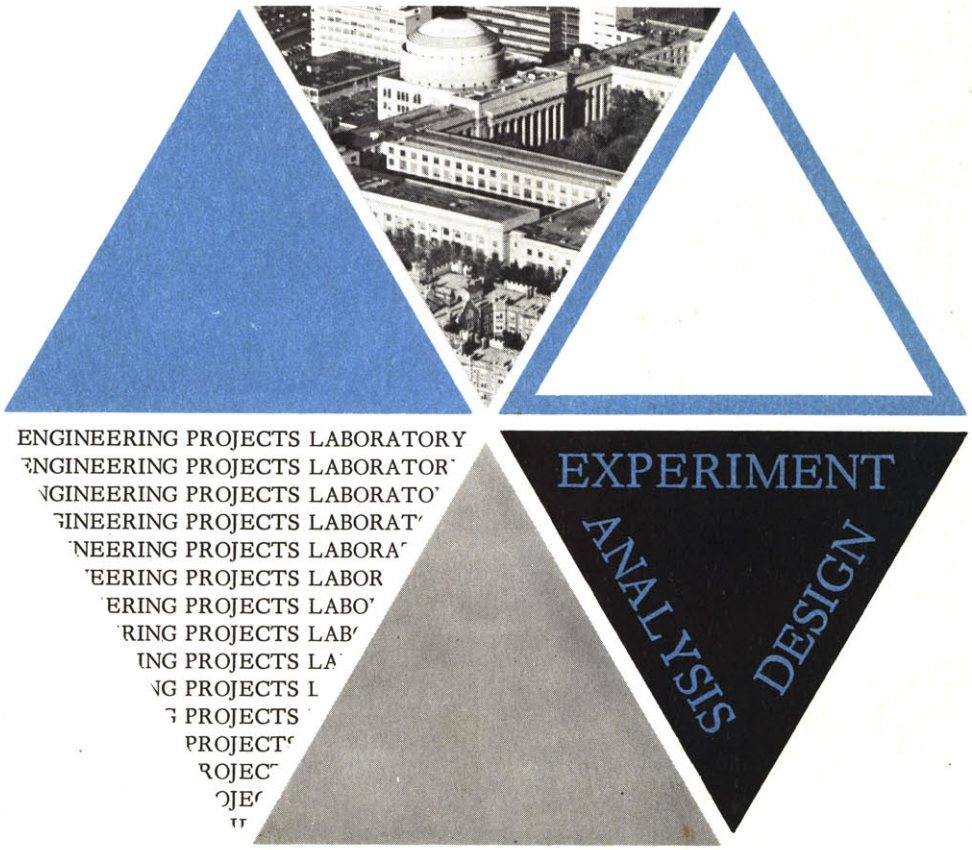

TECHNICAL REPORT NO. 8767-31

PRESSURE DROP WITH SURFACE BOILING IN SMALL-DIAMETER TUBES

by

Thomas Dormer, Jr.

Arthur E. Bergles

for

Massachusetts Institute of Technology

National Magnet Laboratory

Sponsored by the Solid State Sciences Division

Air Force Office of Scientific Research (OAR)

Air Force Contract AF 19(604)-7344

D.S.R. Project No. 8767

September 1, 1964

Department of Mechanical Engineering

Massachusetts Institute of Technology

Cambridge 39, Massachusetts

ABSTRACT

Pressure drop for water flowing in small-diameter tubes under isothermal, nonboiling, and surface-boiling conditions was investigated.

Experimental results for local pressure gradient and heat-transfer coefficients are presented. Heat-transfer results for nonboiling and surface boiling are in agreement with previous investigations. Isothermal friction factors compare favorably with conventional smooth-tube data. Nonboiling friction factors were well correlated with a wall-to-bulk fluid viscosity ratio. It is concluded that boiling pressure gradients cannot be correlated on the basis of local conditions alone. The axial build up of nonequilibrium vapor in the tube produces an increase in pressure gradient even when all other local parameters are constant. The heat-transfer - pressure-gradient analogy was investigated in the boiling region. For the chosen boiling-to-nonboiling ratios, the analogy was found to be valid only under limited conditions.

Over-all pressure-drop data are presented for numerous geometries and a range of flow conditions. Diameters of 0.062 to 0.180 in. and L/D's of 25 to 200 were considered. Exit pressures ranged from 30 to 80 psia and velocities ranged from 5 to 50 ft/sec. The majority of the data was taken for an inlet temperature of 80 °F. Heat fluxes were increased from zero to near the burnout condition unless the saturation condition was reached first. These results were correlated by a relation which is independent of all parameters except geometry. This correlation is presented graphically for all the geometries used. Either this plot or the original data plots can be readily used for design purposes.

ACKNOWLEDGMENTS

This study was supported by the National Magnet Laboratory of the Massachusetts Institute of Technology. The Laboratory is sponsored by the Solid State Sciences Division of the Air Force Office of Scientific Research.

The personnel of the Heat Transfer Laboratory assisted with construction details. The National Magnet Laboratory staff was especially helpful throughout the research program.

Miss Lucille Blake typed the final manuscript as well as the preliminary reports.

We wish to express our thanks to all concerned.

TABLE OF CONTENTS

LIST OF FIGURES

NOMENCLATURE

A	=	surface area
c_p	=	specific heat
D	=	diameter
(dp/dx)	=	local pressure gradient
E	=	test section voltage
f	=	friction factor
g_o	=	gravitational constant
G	=	mass velocity
h	=	heat-transfer coefficient
I	=	test section current
k	=	thermal conductivity
L	=	test section length
L_T	=	total boiling length of Eq. (6)
ℓ	=	local boiling length of Eq. (6)
P	=	absolute pressure
q	=	rate of heat transfer
(q/A)	=	heat flux
q_{sat}	=	heat transfer required to produce saturated exit
R	=	electrical resistance of test section
T	=	temperature
V	=	average velocity
$\bar{V}$	=	mean liquid velocity in Eq. (3)
w	=	mass flow rate
x	=	axial position from inlet

α = constant exponent of Eq. (1)

Δp = overall pressure drop

Δp_{adb} = adiabatic pressure drop

ΔT = temperature difference

ΔT_{sub} = saturation minus bulk temperature difference

μ = dynamic viscosity

ρ = density

Dimensionless Groups*

Nu = Nussult number = hD/k

Pr = Prandtl number = $\mu c_p/k$

Re = Reynolds number = GD/μ

j = $Nu/Re\ Pr^{1/3}$

Subscripts

b = local bulk condition

bo = burnout condition

scb = subcooled boiling condition in Eqs (6) and (7)

ex = exit condition

fc = forced convection

h = heated

in = inlet condition

iso = isothermal

nb = nonboiling condition in Eq. (7)

sat = saturation condition

w = heat transfer surface

x = axial position

---

*Unless otherwise indicated, all properties are evaluated at the fluid bulk temperature

INTRODUCTION

The development of high-performance heat-transfer equipment has stimulated extensive research in boiling heat transfer. Boiling is a practical method of accommodating the high heat-transfer rates characteristic of nuclear reactors and rocket motors. Vaporization of the coolant is frequently desired, for example, in the boiling-water reactor and bootstrap rocket engine. In many other applications, however, the only function of the coolant is to remove heat from the device. The high-field electromagnet, amplitron, and high-temperature pressure transducer are examples. For such applications, the most desirable mode of boiling is subcooled or surface boiling, where the average fluid temperature remains below the saturation point so that vapor formed at the superheated wall condenses when it comes in contact with the colder bulk fluid. The complexities of two-phase flow can then be avoided. Of course, boiling could be eliminated altogether by maintaining sufficiently high coolant velocity. This is often undesirable, however, due to the large-capacity pumping system which would be required.

Space considerations for this high-performance equipment dictate that the coolant passages be of relatively small cross section. Accordingly, a study of the heat-transfer characteristics of small-diameter channels was undertaken in the M.I.T. Heat Transfer Laboratory. The surface-boiling characteristics of smooth tubes as small as 0.047-in. i.d. were found to be similar to the results available for larger diameter channels.[1*] Heat fluxes for stable burnout were found to increase

---

*Numbers refer to References listed beginning on page 46.

substantially as the diameter was reduced below 0.25 in.^{2} The small channels, then, are not only necessary for this equipment but appear to have advantages in general. However, the designer still needs to have information on pressure drop in order to complete the cooling-system design.

Pressure drop in the area of interest is generally separated into two categories: first, pressure drop with forced-convection heat transfer; and second, pressure drop with local boiling up to the point of bulk boiling. Under high-heat-flux nonboiling conditions, pressure drop is chiefly affected by the changes of fluid properties in the boundary layer. Data for turbulent flow of liquids have usually been correlated by an equation of the form

$$f/f_{iso} = (\mu_w/\mu_b)^{\alpha} \qquad (1)$$

where f is the friction factor with heating, f_{iso} the isothermal friction factor at the bulk conditions of the fluid, and μ_w and μ_b are the dynamic viscosity at the wall and bulk temperature, respectively. The exponent α is an empirically determined constant. Seider and Tate,^{3} who first proposed the correlation, used a value of 0.14 for α . Several other investigators have also obtained the same value for this exponent; however, values of 0.25 and 0.3 have also been reported for various liquids.

In most cases, the non-isothermal friction factor used in these correlations is based on total pressure drop. There is evidence that correlation would be improved if only the frictional pressure drop were used. A correction for the acceleration of the fluid due to bulk density

changes must then be made. For example, Rohsenow and Clark[4] correlated total pressure drop data using an exponent of 0.14, but for frictional pressure drop alone the value of α was 0.60. Owens and Shrock[5] used this method and obtained an equation of the form of Eq. (1) with $\alpha = 0.4$. Maurer and LeTourneau[6] obtained data for pressure drop of water in heated rectangular channels, and correlated these data and other data for air by the equation

$$f/f_{iso} = (\mu_w/\mu_b)^{0.25} (\rho_w/\rho_b)^{0.5} \qquad (2)$$

They obtained better correlation by replacing the viscosity exponent (0.25) by the value 10 f_{iso}.

The second region to consider is that of local boiling. When the temperature of the heat-transfer surface is somewhat higher than saturation, vapor bubbles begin to form at the wall. The initiation of boiling occurs first near the downstream end of a channel with forced circulation because of the higher fluid temperature and lower pressure. The agitation of the bubbles increases the heat-transfer coefficient and also increases the pressure gradient in the channel. There may or may not be an increase in the total pressure drop in the tube depending on the condition in the remainder of the tube. With increasing heat flux, surface boiling develops throughout the tube, and the over-all pressure drop will increase.

Early studies have provided data on the effect of local boiling on pressure drop. In one of the earliest studies, Kennel[7] presented data for a heated annulus which indicated that higher heat flux and lower bulk subcooling increased the pressure drop at constant velocity.

Jens and Lottes[8] analyzed pressure-drop data for high-pressure systems and found similar effects. Limited data for small-diameter tubes were presented by Weiss.[9] However, these studies were too specialized to permit predicting pressure drop under other conditions.

Pressure-drop correlations have been proposed based on the heat-transfer pressure-drop analogy. Sabersky and Mulligan[10] were among the first to suggest the extension of the Reynolds analogy to local boiling. They obtained the following equation:

$$\frac{h}{\rho c_p \bar{V}} = -\frac{1}{2}\left(\frac{dp}{dx}\right)\frac{w^{1/2}}{\rho^{3/2}\pi^{1/2}\bar{V}^{5/2}} \tag{3}$$

The data which were approximately correlated by this equation approximated the Reynolds-analogy condition that the Prantdl number be near unity.

Jicha and Frank[11] presented another correlation which relies heavily on the analogy. Their equation is

$$f/f_{iso} = a + b\,j + c(Re) \tag{4}$$

where j is the heat-transfer parameter defined as

$$j = (Nu)/(Re)(Pr)^{1/3} . \tag{5}$$

Values of the pressure-dependent constants a, b, and c were determined by an analysis of their data.

The validity of the analogy correlations is rather questionable for low subcooling where the void fraction is appreciable. The fluid acceleration greatly increases the pressure drop whereas the heat transfer does not seem to be affected.

The effect of vapor voids on pressure drop has been investigated. Miller[12] carried out a photographic study to determine void volumes in a high-pressure system. The void volume was shown to be particularly sensitive to both the bulk subcooling and the heat flux. This void fraction increases sharply as saturation is approached. The measured voids were used to correct the over-all pressure drop so as to obtain the pressure drop due to friction alone.

More recently Costello[13] investigated the void fraction in a low-pressure system. The effects of subcooling, velocity, and heat flux were investigated and a correlation obtained for a narrow range of variables. Costello also emphasized the importance of vapor clotting. The coalescence of vapor bubbles can readily occur in low-pressure systems at low subcooling. Under these conditions, the pressure gradient increases substantially.

Extensive void measurements would enable one to correlate, perhaps by the analogy technique, the frictional pressure drop for surface boiling. However, this separation of the pressure-gradient components appears to be unnecessary since both momentum and friction are functions of all the system variables.

Reynolds[14] measured local pressure gradients for subcooled boiling in a tube. Wall temperatures were also measured so that the point of inception of boiling could be located. The ratio of the boiling-to-isothermal pressure gradients was found to be a function of the ratio of the local boiling length to the total boiling length and the heat flux. A single equation was obtained

$$\frac{(dp/dx)_{scb}}{(dp/dx)_{iso}} = \cosh\left[(4.6 \times 10^{-6}\,(q/A) + 1.2)\,\ell/L_T\right] \qquad (6)$$

which approximately represents data for tubes of 3/8-in. i.d., a velocity range of 7 to 10 ft/sec, a pressure range of 45-100 psia, and a heat-flux range of 1×10^5 to 3×10^5 BTU/Hr-ft^2.

Owens and Schrock[5] conducted similar tests with two smaller test sections. Their data included velocities of 3 to 10 ft/sec., pressures of 50 to 400 psia, and heat fluxes of 2 to 12 x 10^5 BTU/hr-ft^2. They obtained a correlation of the boiling-to-nonboiling pressure gradient as an exponential function of only the local-to-total boiling length ratio,

$$\frac{(dp/dx)_{scb}}{(dp/dx)_{nb}} = 0.97 + 0.028\, e^{6.13(\ell/L_T)} \quad . \qquad (7)$$

The results of Reynolds and Owens and Schrock should be applicable to tubes operating with subcooled exit, providing the total boiling length is properly calculated. However, due to the fact that these investigators always exited at saturation, their heat fluxes were limited to rather low values. The validity of the proposed correlations is therefore somewhat in doubt for conditions of high heat flux. The extension of these correlations to other pressures, velocities, and geometries is also questionable.

The major factors which influence surface-boiling pressure drop have been indicated by these previous experiments. However, at the beginning of this investigation, design data were not available for the low-pressure, small-diameter channels which are required for numerous

high performance heat-transfer devices. Accordingly, an experimental program was undertaken to determine the pressure-drop characteristics of channels less than 0.2-in. i.d. using water at less than 100 psia as the working fluid.

EXPERIMENTAL APPARATUS

Flow Loop and Power Supply

The flow loop used in the experimental program was one already in operation at the M.I.T. Heat Transfer Laboratory. This facility is shown schematically in Fig. 1. It was a closed-loop system in which all components are of corrosion-resistant materials. The system contained the main circulating pump; an accumulator; the test-section line with parallel flowmeters, preheater, test section and its instrumentation; the by-pass line; and a heat exchanger utilizing city water. Auxiliary equipment included a fill pump, supply tank, degassing tank, and a continuous demineralizer. The test-section power was supplied by an a.c. motor-d.c. generator set. A brief description of the major components follows; more detailed information is given in Reference (1).

The main circulating pump was a two-stage, turbine-type pump driven by a 3 hp induction motor. It provided a head of 260 psi at 3.6 gpm. A bladder-type accumulator, pressurized with nitrogen, located at the pump exit served to damp out pressure fluctuations. The ball valve in the bypass line was used to control the bypass flow rate and pressure, which in turn determined the pressures in the test-section line. The test-section line contained two Fischer-Porter flow meters in parallel and the preheater. The preheater was a 5 kw emersion unit fabricated in a 3-in. copper tube and provided with 0 to 100 percent control by a Powerstat auto-transformer.

The test-section power was supplied by motor-generators. The generators were driven by 440-v, 3-phase synchronous motors. Two

36-kw d.c. generators, each nominally rated at 12 v and 3000 amp were connected in series. The generators were provided with water-cooled shunts in parallel with the test section which allowed them to be run open-circuited at the test section either for starting, or after burnout.

Instrumentation

Instrumentation was available for reading pressure levels, differential pressure, temperature, test-section flow rate, and test-section voltage and current. Pressure levels were read on bourdon-tube gages as shown in Fig. 1. At the test-section inlet and exit were 200 and 100 psi test gages with a specified accuracy of $\pm$ 1/4 percent of full scale. These units were also calibrated on a dead-weight tester to an accuracy of approximately $\pm$ 0.1 psi over the full range.

Test-section flow rate was determined from the larger Flowrator meter which had interchangeable tubes and floats. The ranges covered were 20-160, 35-400, and 140-1360 lb/hr. All units were calibrated as installed in the system.

The power supplied to the test section was obtained from the test-section voltage and current. The voltage was read directly on a Weston multiple-range d.c. voltmeter with a specified accuracy of $\pm$ 1/2 percent. The current was determined from a standard shunt with a calibration of 60.17 amp/mv.

All temperatures were measured with copper-constantan thermocouples made from 30-gage duplex wire. The fluid bulk temperature at the inlet and exit of the test section was measured by inserting thermocouples

directly into the fluid using Conax fittings with lava sealants. Methods for measuring wall temperatures are described later. The output voltages of the thermocouples and the shunt were displayed on a continuous recorder. The recorder was a Brown, single-channel instrument having ranges of 0-6, 5-11, 10-16, 15-21, and 20-26 mv.

The manometer system used to measure differential pressures is shown schematically in Fig. 2. It consists of two Meriam 60-in. U-tube manometers, manifolds and valves, and connecting lines of rubber hose. The system was built to read on either manometer a maximum of 10 pressure differences with either one or two reference points. One manometer was filled with mercury which gave a maximum range of approximately 25 psi. The other manometer contained an oil with a specific gravity of 2.00 which allowed a maximum pressure difference of approximately 2 psi. A typical test section with six pressure taps is shown in Fig. 2. The pressure drop from reference "A" (test section inlet) to points 1, 2, 3, 4, and 5 could be read on either the mercury or oil manometers depending on the magnitude of the pressure drop. The two pressure gages were connected to the inlet and exit to give the pressure level and a check on the pressure drop. Vents were included so that all lines could be purged of air.

Test Sections

Two types of test sections were used in this study, each with a specific purpose. The first type was designed to measure pressure gradients along the axis of the tube, while simultaneously measuring the heat transfer. The second type of test section allowed measurements of only the over-all pressure drop.

Pressure-Gradient Test Section

The pressure-gradient test section as used in its final form is shown in Fig. 3. Two test sections with six pressure taps and five wall thermocouples were constructed with virtually identical geometries. These are designated as T.S. 30 and T.S. 31. An earlier test section containing five pressure taps and four wall thermocouples was built and used briefly; however, its construction proved to be too delicate. It is designated as T.S. 20. The complete dimensions of these three test sections are given in Table I.

The tube used for construction of the pressure-gradient test section was of 304 stainless steel with an inside diameter of 0.094 in. Stainless-steel pressure tap tubes (0.028 in. o.d.) were silver brazed on the outside of the tube. The inside of these small tubes was filled with milk of magnesia prior to brazing to prevent their being plugged. The excess braze was then filed away to give a very small fillet at the test section. This completed, the milk of magnesia was removed from the inside of the pressure-tap tube, and a No. 80 drill (0.0135 in.) was used to drill the pressure-tap hole through the test-section tube. Any burrs inside the tube were removed with fine emery cloth and pieces of steel wool pushed through the tube. The power lugs were then soldered in place.

Thermocouples were then attached to the test-section wall. Since d.c. heating was used, a layer of high-temperature teflon tape was applied to the wall for insulation. The thermocouple junction was placed perpendicular to the tube axis, and the lead wires wrapped

around the tube several times and taped in place. Several inches of the lead wire were also left inside the heated shield.

The brazed joint between the test section and pressure-tap tube was rather delicate. In order to provide added rigidity, a piece of high-temperature, fiber-reinforced plastic was cut to fit closely over the pressure-tap tubes and wall thermocouples. It was cemented into place with high-temperature epoxy at each pressure tap. It was necessary to cut this strip into smaller sections because of the different thermal-expansion properties of the plastic and the test-section tube. With the plastic strip in place, extensions of 1/16-in. o.d. stainless tubing were brazed to the pressure-tap tube. Milk of magnesia was used to keep the lines from plugging.

The guard heaters were the last items to be assembled onto the test section. These were made from 1-1/2-inch diam. aluminum tube, which had a shallow thread cut on the outside and a slot cut to fit over the pressure taps. The aluminum was anodized to provide electrical insulation. It was mounted on the tube with lava spacers, the insulation packed inside the heater, and then the chromel heating wire wound in the grooves. More insulation was put around the outside of the heater. Thermocouples were taped to the inside wall of the guard heater. During operation, the power to each guard heater was controlled by variacs so that the temperatures of the heater and the outer wall of the test section were identical.

Prior to installation, the test section was given a final internal cleaning with acetone. Installation in the loop was then the final

step. The power clamps served also as the main support of the test section. The upstream clamp was rigid, and the downstream clamp had axial flexibility to allow for thermal expansion. The test section was horizontal in all cases. The hydraulic connections at the inlet and exit to the test section were Conax fittings with teflon sealants. Both locations had thermocouples to measure bulk fluid temperature. All thermocouples were soldered to a selector switch which was connected so that readings could be noted on either a recorder or a potentiometer. A needle valve was located immediately upstream of the test section to control the flow rate. Stability was assured by maintaining a large pressure drop across this valve, thus isolating the test section from the rest of the system.

Lengths of highly flexible tygon tubing were initially tried for the final connections from the manometers to the pressure taps. The temperature and pressure conditions, however, made this unsuitable. It was finally necessary to use reinforced rubber tubing for these lines. However, due to the limited flexibility, it was necessary to securely mount the lines from the manometer and then complete the connections by soft soldering. A detail of this final connection is shown in detail B of Fig. 3.

Over-all Pressure-Drop Test Section

In addition to the test sections described, simpler ones were constructed for the purpose of measuring over-all pressure drop over the heated length. Thus, these test sections had only two pressure taps and power lugs. Numerous geometries were used, and a complete list

of the dimensions is given in Table II. Four diameters were used with various lengths. For identification, the test sections were coded as follows: The first letter identifies the inside diameter of the tube ("A" -- i.d. = 0.094 in., "B" -- i.d. = 0.1805 in., "C" -- i.d. = 0.121 in., and "D" -- i.d. = 0.062 in.); the number gives the nominal length of the tube in diameters; and the final letter gives the sequence of the test sections of that size built. Thus the identification B100(a) signifies that this test section had an inside diameter of 0.1805 in., a length-diameter ratio of 100, and was the first one built with those dimensions. The largest tube (0.1805 in.) was thin-walled "A" nickel, the 0.094-in. tube was 304 stainless-steel needle tube, and the other two (0.120, 0.062 in.) were 304 seamless stainless-steel tubes.

Two types of static pressure taps were used in the test sections. Differing only in construction, both types performed equally well. Details of the construction are shown in Fig. 3. The first type was the same as those used in T.S. 30 and 31, with the small tube brazed to the larger tube, and then the hole drilled. As before, much of the excess braze was filed away, but in this case the bushing for the power input was adjacent to the tap, and the tube could be soldered to it in order to give the necessary support. A larger 1/16-in. diam. tube was also brazed to the small tap tube. The manometer and pressure-gage lines were connected directly to the 1/16-in. tube with Conax fittings. Milk of magnesia was again used to help prevent the pressure tap from being plugged by braze or solder. The second type of pressure tap was made directly through the power bushings. In this case the pressure-

tap hole was drilled first. The bushing was put in place with the hole directly over the pressure-tap hole and brazed. The 1/16-in. diameter tube was soldered to the bushing. During both steps, extreme care was needed so as not to plug the pressure tap. With either type of construction, the inside of the test section was thoroughly cleaned with emory cloth and steel wool after installation of the pressure tap.

There was no great advantage of one type of construction over the other. The first type did have the advantage of having the heated length of the tube being very nearly the same as the pressure-tap length. This arrangement could not be used with the thick wall tubes ("C" and "D), however, because of the difficulty of drilling the holes in the tube. The other method allowed a larger hole ($\simeq$ 0.030 in.) to be drilled most of the way through the tube, and the small drill the remainder of the way.

The installation of the test sections was essentially the same as for the others. The test section was supported by the power connections which clamped onto the bushings. Inlet and exit fluid connections were through Conax fittings into a tee which also had a thermocouple gland to measure fluid bulk temperature. Immediately upstream of the test section was the needle valve. Since the upstream end of the test section was electrically grounded by the piping, the downstream and the pressure taps were electrically insulated from the loop with rubber hose.

PRESSURE-GRADIENT HEAT-TRANSFER STUDY

Operation Procedure and Data Taking

After installation of the test section, the loop was filled with distilled water, and all lines vented to remove air. The degassing operation was then initiated by heating the water in the degassing tank. With the water boiling, the loop water was heated and slowly sprayed into the top of the tank. Previous experience indicated that half an hour of such degassing reduced the dissolved-air content to approximately 1 cc/liter. After degassing, the heat-exchanger cooling water was turned on to bring the system to normal temperature. The loop was then ready for operation, circulating distilled, deionized, and degassed water.

The general procedure of data taking was to hold the desired flow conditions constant while increasing the heat flux. First, mass flow rate, inlet temperature, and exit pressure level were set with no power to the test section. At this condition the five pressure differences, from the first (inlet) pressure tap to each of the five other taps along the tube, were read separately on the appropriate manometer. The power was then turned on and increased to the first heat-flux level. While the other conditions were maintained, the guard-heater power was adjusted to the balance point; i.e., where the average guard-heater temperature (two thermocouples) was the same as the average outer tube-wall temperature (two or three thermocouples). These temperatures could not be kept exactly equal, but were maintained to within $\pm$ 5 $^{\circ}$F of each other. At equilibrium, wall temperatures, fluid temperatures, pressures,

pressure differences, and test-section voltage and current were recorded. The heat flux was then increased to the next level and the process repeated.

After the highest heat flux was completed, the power was reduced and the exit pressure and/or inlet temperature changed. If only pressure was changed, the power was reduced to the point of incipient boiling. Readings were then taken for a set of heat fluxes at the new pressure. However, if the temperature was changed, the process was repeated completely from a zero-power condition. The procedure was valid since it was verified that the pressure level had no effect on heat transfer or pressure drop in the nonboiling region.

An extensive range of variables was covered in this investigation. The maximum attainable heat flux for any given run was determined by burnout. The burnout heat flux was estimated from data presented in Reference (2) or from data taken in this study. It was desired to approach, but not reach, burnout. However, high heat fluxes were needed, and one test section of this type was lost. The temperature and pressure ranges were largely determined by the system. Beginning at the lowest inlet temperature obtainable, the temperature was increased in increments of 20 ^{o}F up to the maximum temperature that could be achieved with the preheater. With the lowest exit pressure at the test section as a base, pressure increments were chosen so that the saturation temperature increased by 20 ^{o}F. A wider range of mass velocities was obtainable, but it was felt that such data were not necessary.

Data Reduction

The initial data reduction work was done by hand calculation. Later the entire procedure was programmed, and all the data for test sections

30 and 31 reduced by computer. This included computation of local flow and heat-transfer parameters, including flow rate, heat flux, wall superheat, bulk subcooling, pressure gradient, and friction factor as well as the dimensionless groupings Re, Nu, Pr, $Nu/Pr^{.4}$, viscosity ratio, and friction-factor ratio. The mass velocity (G) was determined from the fluid flow rate and tube dimensions. Temperatures were converted from thermocouple emfs with NBS standard calibrations. The heat input was obtained from the tube voltage and current (IE) and checked by the mass flow, specific heat, and temperature rise of the fluid ($wc_p \Delta T$). In the computer calculation, a third value was obtained from the resistance and current (I^2R). The average heat flux was calculated using the several values of heat input. This procedure was valid due to the small axial variation in tube-wall temperature.

Heat-transfer results were based on measurements of the outer wall temperature. A correction for the temperature drop through the tube wall was made to first obtain the inner wall temperature. A modified form of the Kreith and Summerfield[15] solution was used to obtain the necessary correction. This solution assumes an infinite cylindrical resistor, with heat transfer at the inner surface, and an adiabatic outer surface. The final form of the equations as well as thermal-property information is given in Reference (1). At each of the thermocouple positions, calculations were made to obtain local heat-transfer results. The fluid bulk temperature is based on an assumed linear temperature gradient; all fluid properties were obtained from these local bulk temperatures.

The measured gage pressures and pressure differences were used to obtain a pressure-versus-distance equation by a least-squares, curve-fit procedure. This equation then yielded the pressure and the pressure gradient at the desired locations. In these calculations, a cubic equation was used for the curve fitting; however, in some cases the curve fit proved inadequate, and the information was plotted and the gradients obtained graphically. The pressure results yielded the local saturation temperature (T_{sat}), the bulk subcooling ($\Delta T_{sub} = T_{sat} - T_b$), and the wall superheat ($T_{iw} - T_{sat}$). From the pressure-gradient results, the local friction factor and other pertinent values were obtained.

Heat-Transfer Results

Heat-transfer data were required to evaluate the effect of radial temperature gradient on the non-isothermal friction factor. The inception of surface boiling was also established by these data. In addition, the relation between pressure drop and heat transfer was to be checked. The heat-transfer results of this study appear to be in substantial agreement with available data. These results are conveniently split into nonboiling and surface-boiling sections.

The nonboiling results of this study are presented in terms of pertinent dimensionless parameters in Figs. 4 and 5. On the figures are plotted two correlating equations, the lower line being that of McAdams,[16] and the upper one being that obtained from the present data. The present data can be represented by

$$Nu/Pr^{.4} = 0.0157\ Re^{.85}. \tag{8}$$

In Fig. 4 all the data were obtained for $G = 6.67 \times 10^6$ lb/hr ft^2 ($V \simeq 30$ ft/sec); thus the span of Reynolds number results solely from

bulk-temperature variation. Figure 5 presents the results for $G = 4.48 \times 10^6$ lb/hr ft^2 ($V \simeq 20$ ft/sec) and $G = 12.7 \times 10^6$ lb/hr ft^2 ($V \simeq 57$ ft/sec). Comparison of these data shows no particular effect of the mass velocity. An entrance effect is visible in these figures. Thus the data at an L/D of 6, where the thermal boundary layer is still developing, indicate consistently higher heat-transfer coefficients than points further down the tube.

It appears that the divergence from the McAdams correlation is due primarily to the radial property variation which is not properly accounted for in the correlation. This temperature-difference effect was clearly demonstrated in Reference (3) for similar test sections. In any case, the present correlation of Eq. (8) is not suggested as being generally valid. It was devised primarily to facilitate a later comparison between heat transfer and friction.

The present surface-boiling data are shown in boiling coordinates, heat flux vs wall superheat, in Figs. 6 and 7. The first figure presents typical data obtained from the five thermocouples along the wall of the test section. At the lowest heat fluxes, the temperature along the tube steadily increases due to the increase in bulk temperature. At high heat fluxes, the boiling is fully developed, and the wall superheat should be independent of subcooling; however, the temperature profile is seen to be irregular. Generally the highest superheat occurs near the middle of the tube while the ends are colder. The beginning of the tube may be expected to have a somewhat lower temperature due to the entrance effect. The exit condition would appear to be mainly the result of thermocouple errors or conduction losses at the end.

The local data for each run were averaged so as to show more clearly the effects of velocity, subcooling, and pressure. The average boiling curves for different velocities appear to merge for constant pressure. Since a range of subcooling occurs within each run, it can also be concluded that subcooling has little effect on the fully-developed boiling region. These data, then, are in agreement with the usual observation that fully-developed boiling is dependent only on pressure level for a given fluid and surface. Only the highest (80 psia) and lowest (30 psia) pressures are shown in the figures; the data for the other pressures (42 and 57 psia) lie between these.

Pressure-Gradient Results

Isothermal

Prior to heating the tube, isothermal measurements were taken for various temperatures and velocities. An isothermal point was also taken just prior to each boiling run. For such a measurement, all five pressure drops were recorded, and a single pressure gradient was obtained from them. The substantial calming length (> 25D) before the first pressure tap appeared to eliminate any hydraulic entrance effect.

Friction factors were calculated from the isothermal pressure gradients using the standard definition

$$f = -\frac{D}{4}\left(\frac{dp}{dx}\right)\frac{2\rho_b g_o}{G^2} . \qquad (9)$$

Figure 8 gives friction factor versus Reynolds number for these two test sections (T.S. 30 and T.S. 31) and also for a test section with only two pressure taps (T.S. A25). The data generally fall slightly above the Moody smooth-tube correlation as would be expected. The data

of T.S. 31 have considerably more scatter, but have about the same average value as the other test sections. In a later section a correlation for isothermal friction-factor data is needed. The equation used was

$$f_{iso} = 0.107\ Re_b^{-0.28} \qquad (10)$$

and is shown in Fig. 8.

Pressure Drop with Nonboiling Heat Transfer

The friction factor was calculated from pressure gradients obtained in the forced-convection region using Eq. (9) and local bulk fluid properties. As noted in the introduction, the correlation scheme generally used for this region involves a friction ratio as a function of some fluid-property ratio. The ratios chosen for the present study were f/f_{iso} and μ_w/μ_b.

The data from this study are presented in Figs. 9 and 10, using the above ratios as coordinates. The three sections of Fig. 9 give all the data for T.S.'s 30 and 31. These data are calculated from the local pressure gradient and conditions in each of the five sections along the tube. Pressure gradients were obtained by machine computation where a cubic curve was fitted to the pressure-drop data. Data from T.S. 30 can be correlated by

$$f/f_{iso} = (\mu_w/\mu_b)^{\alpha} , \qquad (1)$$

with α equal to 0.35. Data from T.S. 31 (at conditions similar to those of T.S. 30), however, have a large amount of scatter, although a correlation with $\alpha = 0.35$ is approximately correct. These data show

a tendency for f/f_{iso} to increase along the length of the tube, an effect that was not evident previously.

The validity of the curve-fit procedure used in the data reduction was checked by graphically obtaining pressure gradients; a slight improvement in the amount of scatter is noted. Next, it was assumed that the pressure gradient in the tube is linear. A single value of (dp/dx) was used to get f along the tube, while local conditions were used for f_{iso}, μ_w, and μ_b in each section of the test section. A sample of the data of T.S. 31 (covering the full range of variables at 20 ft/sec) was thus analyzed and is presented in the first section of Fig. 10. The correlation with $\alpha = 0.35$ is remarkably good.

The remaining sections of Fig. 10 show some similar pressure-drop data. In this case only the over-all pressure drop in a tube similar to those used above was measured. A linear pressure gradient was assumed, and the average conditions in the tube were used to calculate the wall temperature (from the heat-transfer correlation), the viscosity ratio, and isothermal friction factors. Finally, the results were plotted as before for a wide range of variables. These data also give a good correlation, although the best value for α could be somewhat lower than 0.35.

The data of this study, then, are well correlated by Eq. (1) with $\alpha = 0.35$. This result was obtained for a limited range of variables, however, and in all probability the exponent would vary for different systems depending on the temperature variation of viscosity. The best estimation of the over-all pressure drop is obtained by a stepwise calculation which takes into account the property variation.

Surface-Boiling Pressure Gradient

Figure 11 presents axial pressure profiles for a wide range of boiling heat fluxes at constant velocity. Heat-transfer measurements indicated that the local pressure gradient increased at incipient boiling. Substantial changes in local pressure gradient are noted as the heat flux is increased from incipient boiling to near burnout. It is noted that at very high heat fluxes, the pressure gradient in the first half of the test section has increased only moderately, while at the tube exit it is ten times or more higher.

Some of the variations of pressure gradient which occur are shown in Fig. 12. The left-hand section presents pressure gradient as a function of local subcooling for several pressures and heat fluxes at constant velocity. Inlet temperatures were chosen such that a common range of subcoolings is covered at each heat flux. At a given heat flux and subcooling the axial position is the same for each pressure. For these conditions, the local pressure gradient is seen to be relatively independent of pressure level. The second part of Fig. 12 presents (dp/dx) as a function of ΔT_{sub} for several heat fluxes and one pressure. This time, however, the inlet temperature was varied so that at constant heat flux and subcooling the local pressure gradient is given at several different positions. The pressure level varies somewhat for this plot; however, the preceding plot shows that pressure level is not important. At constant heat flux, subcooling, and pressure, then, local pressure gradient is seen to increase substantially with length.

Clearer evidence of the effect of flow history is given in Fig. 13. The variation of (dp/dx) along the length of the test section is shown

for various values of subcooling and heat flux. In almost every case, for constant local conditions, an axial increase in the pressure gradient is present. This increase in axial pressure gradient can be sttributed to the vapor bubbles which are carried downstream before condensing. The increasing nonequilibrium void volume causes an acceleration pressure gradient which increases with length. These results emphasize that pressure gradient cannot be predicted from local conditions alone; that is, the previous history of the flow affects the pressure gradient.

Heat-Transfer Pressure-Drop Analogy

The data indicated that both heat-transfer coefficient and pressure drop increase with surface boiling. These data were then analyzed to see if an analogy between pressure drop and heat transfer could be derived. The preceding experiments indicated that the analogy would probably be most successful when relatively high subcooling was maintained.

A desirable form of the analogy would give a measure of the effect of boiling on heat transfer and pressure gradient. Ratios were defined for this purpose. These give the ratio of the heat transfer (or pressure drop) present with boiling to the value to be expected without boiling, if all other conditions are the same. The ratios used were

$$Nu/Nu_{fc} = \frac{qD}{A(T_w - T_b)k}/0.0157\ Re_b^{0.85}\ Pr_b^{0.4} \qquad (11)$$

and

$$f/f_{fc} = \frac{D\rho_b g_o}{2G^2}\left(\frac{dp}{dx}\right)/0.107\ Re_b^{-0.28}\left(\frac{\mu_w}{\mu_b}\right)^{0.35}, \qquad (12)$$

where forced convection values are from the correlations of data from this investigation as given by Eqs. (8) and (10).

Figs. 14 and 15 present the results from a representative portion of the local data. On the average, the theoretical 45° line is representative of the data up to a point. However, beyond certain conditions the pressure-drop effect increases much more rapidly than the heat transfer. This condition, which first occurs near the test-section exit, is associated with the production of large vapor fractions. The appearance of a position effect is very pronounced in the figures. At the inlet, the pressure gradient is low, at times lower than predicted for nonboiling forced convection. This is due primarily to the use of average forced-convection correlations in Eqs. (11) and (12). As noted earlier Nu_{fc} was higher and f_{fc} lower in the entrance region. Near the middle of the test section the ratios are approximately equal. At the exit, when large void fractions are present, the pressure-drop effect can be three or four times as large as the heat-transfer effect. Thus, while this analogy may give reasonable values for averaged conditions, the history of the flow is too important a factor to be ignored.

OVER-ALL PRESSURE-DROP STUDY

Purpose and Scope

The previous section has confirmed that it is not possible to present subcooled-boiling pressure gradients purely in terms of local conditions. Gradients, then, offer no particular advantage to the designer since the history of the flow, or equivalently channel length, cannot be eliminated as a variable. Over-all pressure-drop data for a wide range of geometries and flow conditions were considered to be more useful for design.

The independent parameters are temperature, pressure, fluid velocity, heat flux, tube diameter, and tube length. A wide range of these variables was chosen within the limits of the test loop.

For greatest generality the data were limited to the over-all static pressure drop in the heated portion of the test section. The contributions of unheated lengths, entrance effects, and exit effects can be included for the particular application. The first consideration was the selection of test-section geometry. Diameters of approximately 1/8 in. and lengths from 25 to 100 diam. were desired. The tubes listed in Table II were chosen because of availability and compatability with the d.c. power supply.

The fluid velocity at the inlet was varied from 5 to 40 ft/sec. Pressure at the test section exit was set at 30, 50, and 80 psia. An inlet temperature of 75 or 80 ^{o}F was selected as being representative of most cooling equipment. Data for variable inlet temperature were obtained from the previous study of pressure gradients. The heat flux

for each run (one temperature, pressure, and velocity) was varied from zero to near burnout* or until conditions at the tube exit were near saturation. Since every combination of variables could not be tested for every geometry, some were left out. Generally, the high and low pressures were not run for some velocities. With some geometries, only one pressure was run for each velocity.

Operation and Data Reduction

Operation of tests were almost identical to those for the pressure-gradient study. After the test section was installed, the test-section line and manometer lines were vented. The system was then degassed as explained before.

Data taking was again very similar to the first procedure, but much simpler. Isothermal pressure drops were measured for various fluid temperatures and velocities. The data were checked before continuing to ascertain if pressure taps were properly installed. For each heated run, the desired initial conditions (inlet temperature, exit pressure, fluid velocity) were set, zero power readings were made, and then the test-section power increased to give the first heat flux. After equilibrium was reached, readings were made for: flow rate, inlet and exit temperature, tube voltage and shunt voltage (tube current), inlet and exit pressure, and test-section pressure drop. Readings were continued for each heat flux up to the maximum. Then, the next set of initial conditions were set and the process repeated.

---

*The burnout data, which were usually obtained unintentionally, are presented in the Appendix, Table III.

One interesting problem was encountered in obtaining data. This was with the 0.121 in. diam. tubes. The test section appeared to operate normally to the point of first boiling; beyond that point the pressure drop began to increase as expected. However, at higher heat flux, the pressure drop began decreasing again. If allowed to continue, negative pressure drops were actually indicated. The action of the pressure gages indicated the downstream tap to be giving the erroneous results. A second test section gave similar results, as did reversing the manometer connections. Then the test section itself was reversed, so if the pressure taps were at fault, the effect should have been reversed. Essentially the same results were obtained, however.

The trouble was finally attributed to boiling at the edge of, or within, the pressure tap. The thick wall and the high currents combined to produce very high outside wall temperatures while operating. Rough measurements (a thermocouple taped to the tube wall and insulated, but no guard heater) indicated temperatures in excess of 850 ^{o}F; in some cases they may have been close to 1000 ^{o}F. Under these conditions the temperatures at the bushing and pressure tap would have been high enough to produce boiling.

The only satisfactory method of obtaining the data under these conditions was to lower the temperature near the pressure tap by cooling. This cooling was accomplished by intermittently spraying water at the area. Whenever the data were questionable, cooling produced a rapid change in the differential pressure reading. Readings were then made after equilibrium was established with the cooling. In regions which appeared normal (i.e., no boiling in tube), cooling produced no change.

The most difficulty occurred with T.S.'s C25 and C50, where this problem was first observed. Generally all the data, with and without buss cooling, are shown in the figures unless a reading was obviously too low. Because of this overheating, the results in Figs. 22 through 25 are not as reliable as the other results.

Isothermal data were analyzed as described previously. The remaining data were analyzed to obtain pressure drop and heat flux. Pressure drop was converted directly from the manometer readings. Heat flux was obtained from the electrical power and tube dimensions ($E\ I / \pi D_i\ L_h$). The heat input calculated from electrical power checked with the temperature readings and flow rate to within a few percent. The remaining data reduction involved the calculation of the correlating parameters defined below.

Pressure-Drop Data

Isothermal pressure drop was measured for all the test sections used in this study. The data for tubes of i.d. = 0.094 in. were presented in Fig. 8 and discussed previously. Fig. 16 gives representative data for each of the other tube sizes used, i.d. = 0.18, 0.12, and 0.062 in. The larger two tubes give normal results, the data being slightly above the Moody smooth-tube curve, and having an average amount of scatter. However, the data of the smallest tube lie below the Moody line. Results of the three different test sections are consistent within themselves, and have little scatter. Since it is generally agreed that the Moody line should be the lower limit of the data, the most reasonable explanation of this behavior seems to lie in the pressure-tap size.

Rayle[18] recommends static orifices of less than 1/10 the tube diameter so as not to disturb the flow; in this case the orifice was approximately 1/5 the tube diameter.

All the over-all pressure-drop data obtained in this investigation are shown in Figs. 17 through 28. Essentially the data are in a "raw" form, giving pressure drop vs. heat flux, with temperature, pressure, and velocity as independent parameters. Each figure contains data for one geometry. The first data are for diameter "A" (0.094 in.), then for diameters "B" (0.1805 in.), "C" (0.121 in.), and "D" (0.062 in.) in order. The results are given for decreasing L/D ratio for each diameter.

Discussion and Correlation of Results

The results suggest three regions of pressure drop. The first region is that of nonboiling. As the heat flux is increased from zero, the over-all pressure drop decreases until surface boiling begins at the tube exit. The second region begins when the pressure drop increase, due to bubble agitation in the downstream section, balances the decrease due to nonboiling forced convection near the entrance. This second region then continues with a gradual increase in pressure drop. The third region begins as a large nonequilibrium void fraction sharply increases the pressure drop. This steep increase continues without any discontinuity to the point of saturated exit and beyond to the highest exit qualities obtained in this study of approximately 6 or 7 percent.

The appearance and extent of each of the three regions on a pressure-drop - heat-flux plot is influenced chiefly by the length of the tube. For a tube of approximately 50 diam. long (for example, see Fig. 17), the three regions are very distinct. Boiling at the tube exit occurs at high

subcoolings (and high heat flux). The pressure drop increases gradually due to bubble formation and agitation as the heat flux is increased; however, the bubbles condense rapidly without producing high void fraction. This increase then continues for some time before the voids associated with the third region are produced. For a shorter tube (25 L/D, for example) boiling begins at even higher subcooling, and as a result, the range of the second region is extended. However, the associated high heat flux will generally produce burnout before the third region is reached. With longer tubes, boiling will begin at lower subcooling, the second region will become shorter, and the third region will be entered more quickly. Finally, for very long tubes, the first region will continue with decreasing over-all pressure drop until the exit temperature approaches saturation. Then there will be an almost immediate production of high void fraction with a correspondingly large increase in pressure drop.

Except for the above effects of geometry, the pressure-drop - heat-flux curves tend to have a common appearance. This suggests a possible method of correlation. For example in Fig. 17, the effect of increasing inlet temperature is to "compress" the curves, increasing pressure "expands" the curves, while they all have the same general appearance. The effect of velocity is to change the range of heat flux and pressure drop over which a curve extends, but not the shape of the curve. A pair of convenient, non-dimensional parameters was desired for correlation. The ordinate should combine the effects of subcooling and heat flux while the abscissa should account for the velocity effect.

The parameters selected were the following: The pressure-drop parameter, $\Delta p / \Delta p_{adb}$, is the ratio of the actual pressure drop in the heated tube to the pressure drop in a similar adiabatic tube, i.e., a tube with similar geometry and fluid inlet condition, but with no heat addition. The second parameter, q/q_{sat}, compares the actual heat added to the heat addition required to just produce saturated exit conditions. These coordinates have some disadvantages. They were intended primarily for the second and third region of pressure drop, and give some undesirable effects in the first region. For example, with non-boiling pressure drop, pressure level does not affect the results, but will change the parameter q/q_{sat}. However, a correlation previously discussed is intended to cover most of this region.

Figs. 29 through 33 present portions of the correlated pressure-drop data using the parameters discussed. Fig. 29 gives data for one velocity, and various temperatures and pressures. As expected, the correlation is only fair in the first region, but beyond this initial section, correlation is very good. Fig. 30 shows the result of the correlation with various velocities and pressure for a different geometry. A third geometry is presented in Fig. 31 where it is seen that the correlation is again good over a wide range of variables. All the data of this study were similarly treated. In all cases the pressure, velocity, and temperature effects were well correlated by the chosen parameters.

The geometry effects are indicated in Figs. 32 and 33. Fig. 32 presents a comparison of data for three diameters with all other variables remaining the same. In Fig. 33 a single curve was drawn through

the data of each geometry. As shown in Fig. 32 for a length of 100 L/D, the pressure-drop ratio increases with increasing diameter throughout the boiling range. The diameter effect is not definitive, however, since the data for other lengths in Fig. 33 show an occasional reversal of the effect. The increase might be expected initially since incipient boiling is inversely dependent on diameter. However, one would expect the momentum pressure gradient to increase with decreasing diameter due to the greater tendency towards bubble coalescense. In any case the diameter effect is not too substantial. The length is still a most important parameter. Correlation of the length effect would be rather involved since the curves for various lengths are different in shape.

The correlated form of the data as given in Fig. 33 should be of the greatest use to the designer. Although, in some case it would be less accurate than the raw data, it will simplify the problem of multiple interpolations. It will also increase the confidence of extrapolating outside the actual range of the data.

SUMMARY

An experimental program was performed to determine the pressure-drop characteristics of horizontal tubes 0.18 in. i.d. and smaller with water at less than 100 psia. Isothermal, nonboiling, and surface-boiling conditions were investigated over a wide range of fluid temperatures and velocities.

The first part of the experimental program was conducted to simultaneously obtain local heat-tranfer and pressure-gradient data.

Nonboiling heat transfer is given in terms of the appropriate nondimensional parameters and compared with the McAdams equation. The data are slightly higher than the McAdams correlation due to radial property variation. Boiling heat-transfer results are presented in terms of heat flux and wall-to-saturation temperature difference. The heat transfer is dependent on pressure in the fully-developed boiling region, but independent of subcooling and velocity.

Isothermal friction factors compare favorably with conventional smooth-tube data.

Nonboiling friction factors were well correlated with the viscosity ratio

$$f/f_{iso} = (\mu_w/\mu_b)^{0.35} \qquad (1)$$

This result was found valid for various types of pressure-drop measurement and for different techniques of data reduction. Used were measured local pressure gradients and wall temperatures, linearized pressure gradients and measured local wall temperatures, and over-all pressure drop and average wall temperatures calculated from heat-transfer results.

Boiling pressure gradients are presented for a limited range of variables. The effect of pressure, in the range from 30-80 psia, on the local pressure gradient was found to be of minor importance. It is concluded that pressure gradient cannot be predicted from local conditions alone. The build up of nonequilibrium vapor volume along the test section is responsible for this complicating feature.

The heat-transfer - pressure-gradient analogy was investigated in the boiling region. Parameters were defined as boiling-to-nonboiling ratios of Nusselt number and pressure gradient. The analogy was found to be reasonably valid for conditions of high subcooling; however, variations along the axial length limit its acceptability. As would be expected, the relationship becomes invalid at low subcooling due to the large vapor volume.

Since the pressure gradients are dependent on the flow history, or channel length, it was more desirable to take the remaining data simply in terms of over-all pressure drop for the heated section. The data are presented in Figs. 17 to 28 as pressure drop versus heat flux for numerous geometries and a range of fluid conditions. Diameters of 0.062 to 0.1805 in. and L/D's of 25 to 200 were considered. Exit pressures ranged from 30 to 80 psia, and velocities ranged from 5 to 50 ft/sec. The majority of the data was taken for an inlet temperature of 80 ^{o}F, although some variations in inlet temperature are reported. Heat fluxes were increased from zero to near the burnout condition unless the saturation condition was reached first.

A correlation of these data was obtained. The parameters chosen were $(\Delta p/\Delta p_{adb})$, the ratio of the measured pressure drop to the

pressure drop in a similar adiabatic tube with the same inlet conditions, and (q/q_{sat}) the ratio of actual heat addition to that required to produce a saturated exit condition. Using these parameters, the data are independent of all variables except geometry. Tube diameter has a small effect, while the length-diameter ratio is of major importance. A single composite plot is presented in Fig. 33 which gives the relationship of the correlating parameter for all the geometries investigated. Either this plot or the original data plots can be readily used for design purposes.

REFERENCES

1. A. E. Bergles and W. M. Rohsenow, "Forced-Convection Surface Boiling Heat Transfer and Burnout in Tubes of Small Diameter," D.S.R. Report 8767-21, Dept. of Mechanical Engineering, Massachusetts Institute of Technology, May, 1962.

2. A. E. Bergles, "Subcooled Burnout in Tubes of Small Diameter," A.S.M.E. Paper No. 63-WA-182, 1963.

3. E. N. Seider and G. E. Tate, "Heat Transfer and Pressure Drop of Liquids in Tubes," Ind. Eng. Chem., Vol. 28, 1429-1436, 1936.

4. W. M. Rohsenow and J. A. Clark, "Heat Transfer and Pressure Drop Data for High Heat Flux Densities to Water at High Sub-critical Pressures," 1951 Heat Transfer and Fluid Mechanics Institute Preprints, Stanford University Press, 1951.

5. W. L. Owens and V. E. Schrock, "Local Pressure Gradients for Subcooled Boiling of Water in Vertical Tubes," A.S.M.E. Paper No. 60-WA-249, 1960.

6. G. W. Maurer and B. W. LeTourneau, "Friction Factors for Fully Developed Turbulent Flow in Ducts with and without Heat Transfer," A.S.M.E. Paper No. 63-WA-98, 1963.

7. W. E. Kennel, "Local Boiling of Water and Superheating of High Pressure Steam in Annuli," Sc.D. Thesis in Chemical Engineering, Massachusetts Institute of Technology, 1948.

8. W. H. Jens and P. A. Lottes, "Analysis of Heat Transfer, Burnout, Pressure Drop, and Density Data for High Pressure Water," Argonne National Laboratory Report 4627, May 1, 1951.

9. D. H. Weiss, "Pressure Drop in Two-Phase Flow," Argonne National Laboratory Report - 4916, Oct. 1952.

10. R. H. Sabersky and H. E. Mulligan, "On the Relationship Between Fluid Friction and Heat Transfer in Nucleate Boiling," Jet Propulsion, 25, #1, 9-12, 1955.

11. J. J. Jicha and S. Frank, "An Experimental Local Boiling and Pressure-Drop Study of a Round Tube," A.S.M.E. Paper No. 62-HT-48, 1962.

12. M. L. Miller, "Pressure Drop in Forced-Circulation Flow of Subcooled Water with and without Surface Boiling," S. M. Thesis in Mechanical Engineering, Massachusetts Institute of Technology, Aug. 1954.

13. C. P. Costello, "Aspects of Local Boiling Effects on Density and Pressure Drop," A.S.M.E. Paper No. 59-HT-18, 1959.

14. J. B. Reynolds, "Local Boiling Pressure Drop," Argonne National Laboratory Report 5178, March, 1954.

15. F. Kreith and M. Summerfield, "Investigation of Heat Transfer at High Heat Flux Densities: Experimental Study with Water of Friction Factor with and without Surface Boiling in Tubes," Jet Propulsion Lab. C.I.T. Progress Report No. 4-68, 1948.

16. W. H. McAdams, et al, "Heat Transfer at High Rates to Water with Surface Boiling," Industrial and Engineering Chemistry, Sept. 1949.

17. A. P. Colburn, "A Method of Correlating Forced Convection Heat Transfer Data and a Comparison with Fluid Friction," Trans. A.I.Ch.E., Vol. 29, 177-220, 1933.

18. R. E. Rayle, "Influence of Orifice Geometry on Static Pressure Measurements," A.S.M.E. Paper No. 59-A-234, 1959.

19. W. M. Rohsenow and H. Y. Choi, Heat, Mass, and Momentum Transfer, p. 58, Prentice-Hall, Inc., Englewood Cliffs, N. J., 1961.

APPENDIX

TABLE I

Dimensions of Pressure-Gradient Test Sections

Tube: Type 304 Colddrawn Stainless Steel

o.d. = 0.120 in. i.d. = 0.094 in.

Test Section Identification	Calming Length	Heated Length	Distance to Pressure Taps	Distance to Thermocouples	
T.S. 20	2.00 in.	4.66 in.	0	.58 in.	6 D
	21 D	50 D	1.25 in.	1.75	19
			2.41	2.91	31
			3.55	4.05	43
			4.80		
T.S. 30	3.02 in.	4.90 in.	0	.61 in.	6 D
	32 D	52 D	1.22 in.	1.84	20
			2.47	2.97	32
			3.47	3.83	41
			4.20	4.57	49
			4.95		
T.S. 31	3.10 in.	4.90 in.	0	.61 in.	6 D
	33 D	52 D	1.22 in.	1.84	20
			2.46	2.97	32
			3.46	3.83	41
			4.23	4.57	49
			4.96		

TABLE II

Dimensions of Over-All Pressure-Drop Test Sections

Test-Section Identification	Heated Length (in.)	Heated Length (L/D)	Pressure-Tap Length (in.)	Pressure-Tap Length (L/D)	Calming Length (in.)	Calming Length (L/D)
	Tube "A" Type 304 Stainless Steel					
	i.d. = 0.094 in.		o.d. = 0.120 in.			
T.S. 21	4.62	49	4.84	52	2.40	25
T.S. 22	4.53	48	4.81	51	2.4	25
T.S. 23	4.59	49	4.86	52	2.4	25
T.S. 25	4.62	49	4.82	51	2.4	25
T.S. 30	4.90	52	4.95	53	3.02	32
T.S. 31	4.90	52	4.96	53	3.10	33
A25 (a)	2.30	24	2.33	25	2.31	25
A25 (b)	2.30	24	2.34	25	2.37	25
	Tube "B" Type "A" Nickel					
	i.d. = 0.1805 in.		o.d. = 0.211 in.			
B100 (a)	18.0	100	18.08	100	4.75	26
B 50 (b)	9.06	50	9.06	50	4.6	25
B 50 (b)	8.90	49	9.02	50	4.6	25
B 25 (c)	4.41	24	4.52	25	4.49	25
	Tube "C" Type 304 Stainless Steel					
	i.d. = 0.121 in.		o.d. = 0.250 in.			
C150 (a)	17.86	147	18.00	148	3.18	26
C100 (a)	11.85	98	11.97	99	3.06	25
C 50 (a)	5.87	48	5.99	49	3.07	25
C 50 (b)	5.90	49	6.00	49	3.0	25
C 25 (a)	2.92	24	3.00	25	3.0	25
C 25 (b)	2.85	24	2.99	25	3.05	25
	Tube "D" Type 304 Stainless Steel					
	i.d. = 0.062 in.		o.d. = 0.125 in.			
D200 (a)	12.06	195	12.20	197	2.75	46
D150 (a)	9.00	145	9.13	147	2.75	46
D100 (a)	5.94	96	6.08	98	2.75	46

TABLE III

Burnout Data

Identification	D (in.)	L/D	$V_{in.}$ (Ft/Sec)	P_{ex} (psia)	ΔT_{sub} (^{o}F)	x_o (%)	$(q/A)_{bo} \times 10^{-6}$ Btu/Hr Ft^2
BO-30-1	0.094"	49.9	40	30.0	50	-	5.72
BO-30-2	"	49.9	40	30.0	32	-	5.58
BO-30-3	"	49.7	40	30.0	10	-	5.48
BO-30-4	"	50.0	40	30.0	0	-	5.42
BO-30-5	"	50.1	21	30.0	17	-	3.88
BO-30-6	"	49.9	21	30.0	-	0.2	3.88
T.S. 21	"	49.2	40	30.0	82	-	4.99
T.S. 22	"	48.2	40	29.0	77	-	4.98
T.S. 23	"	49.0	10	30.3		0.1	2.13
T.S. 30	"	52.2	30	80	79		4.45
B50 (a)	0.1805	50.2	10	50	29	-	1.78
B25 (c)	"	24.5	30	50	108	-	4.76
C50 (a)	0.121	48.5	20	50	56		3.52
C50 (b)	"	48.7	30	50	70		4.42
C25 (b)	"	23.5	10	50	68		3.51
D200 (a)*	0.062	195	20	78	4		1.26

*Burnout could have been caused by compressible-volume induced oscillation from pressure instrumentation.

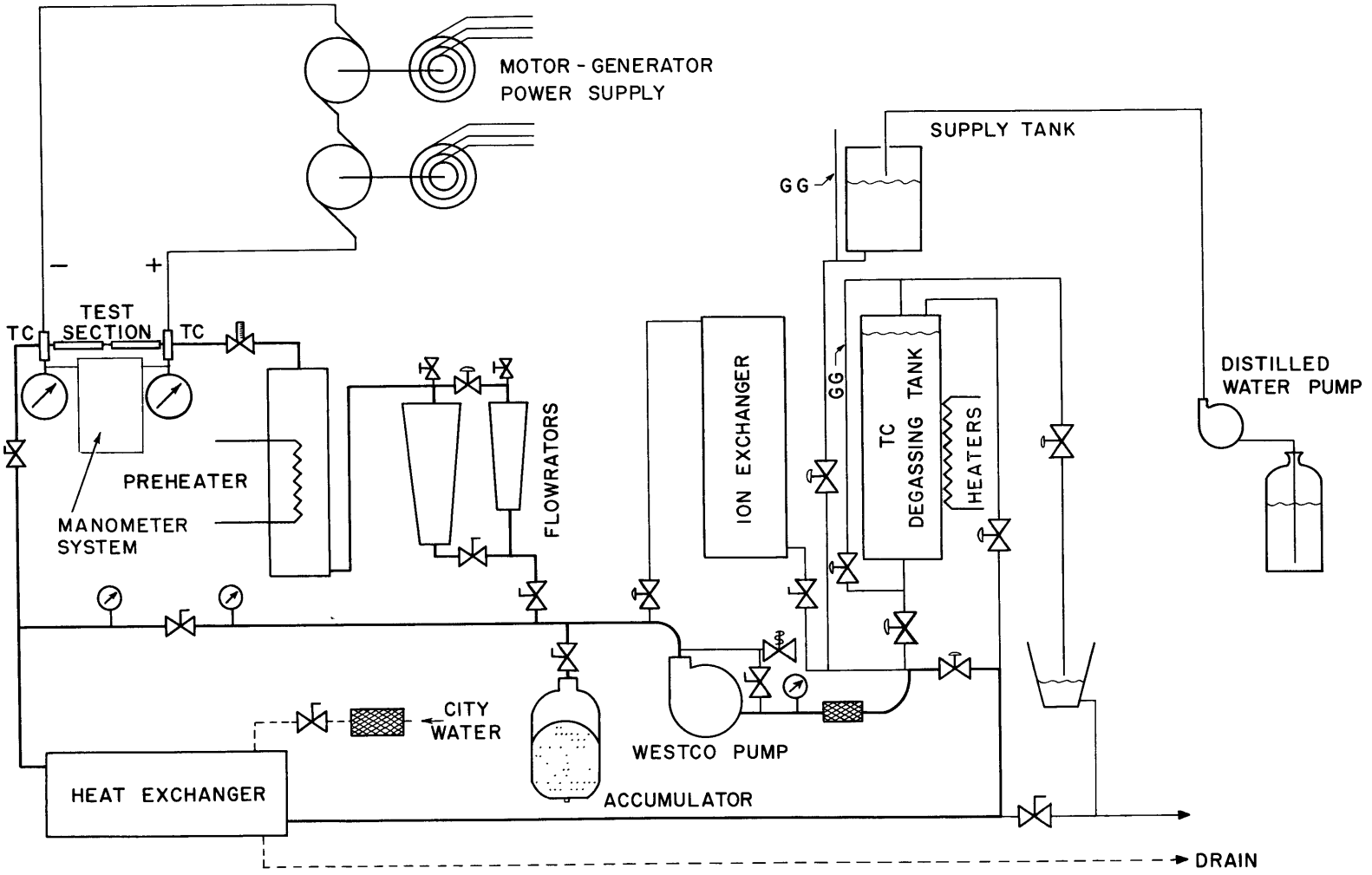

FIG. 1 SCHEMATIC LAYOUT OF EXPERIMENTAL FACILITY

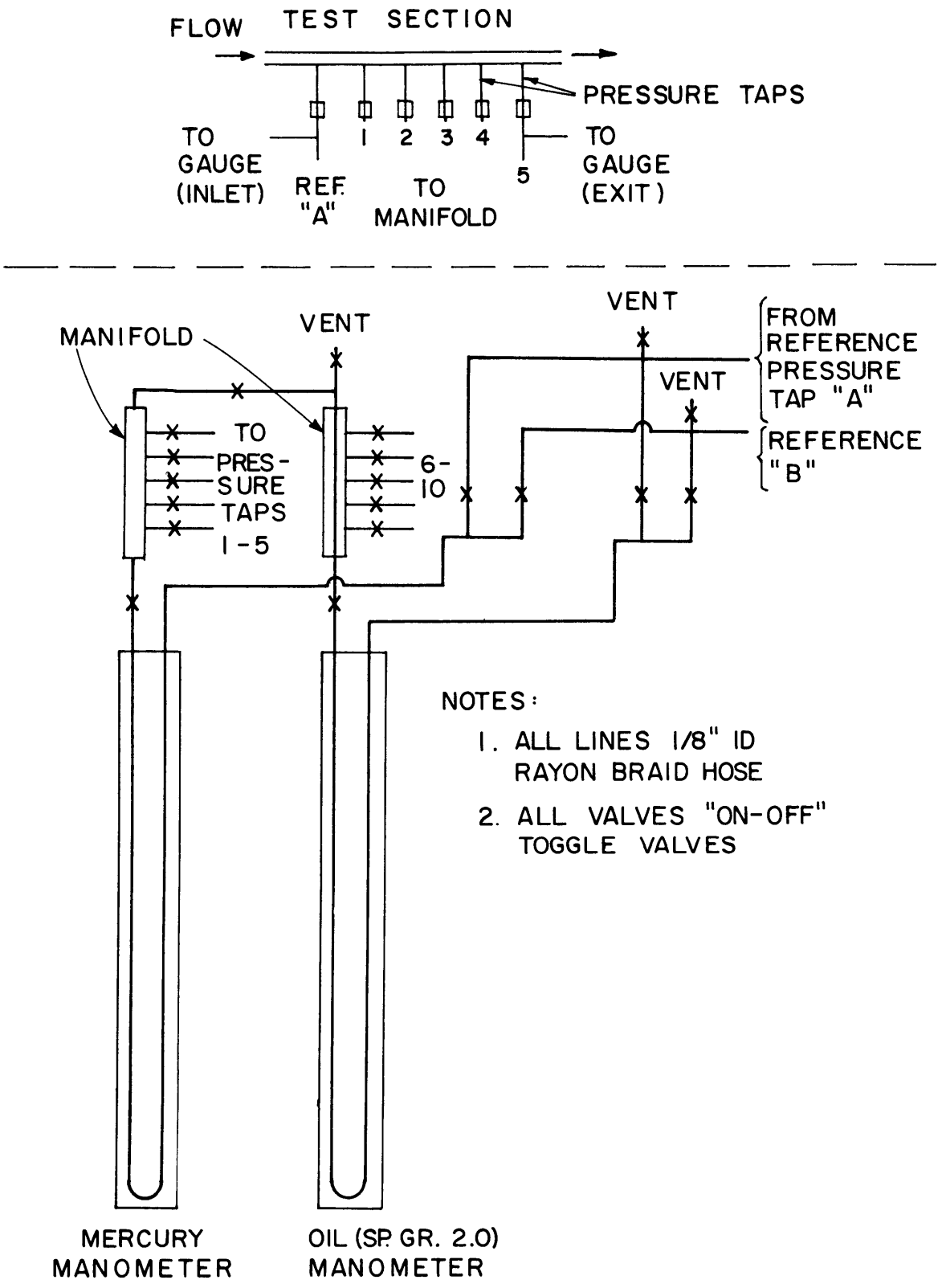

FIG. 2 SCHEMATIC OF MANOMETER SYSTEM

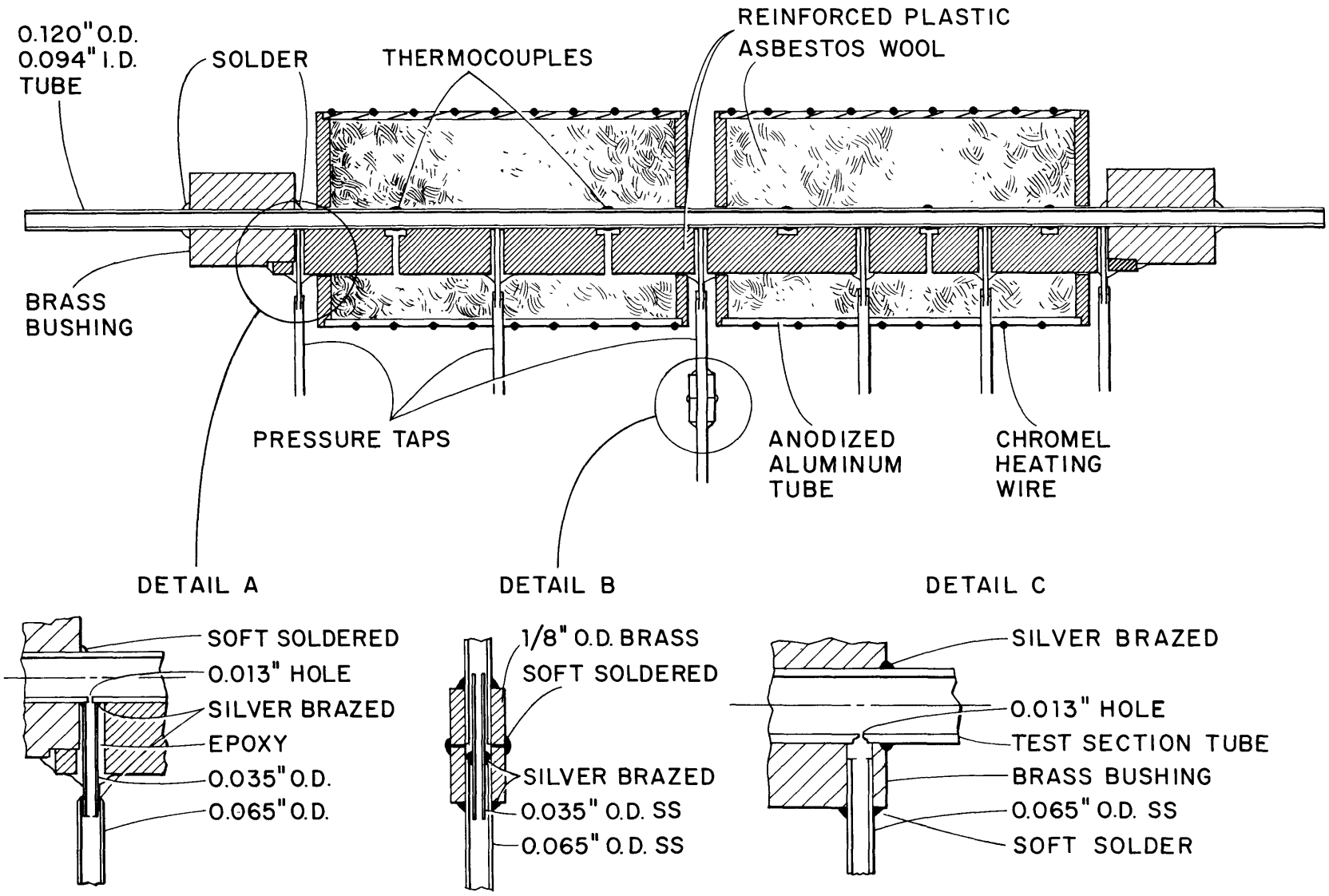

FIG. 3 DETAILS OF TEST SECTION CONSTRUCTION

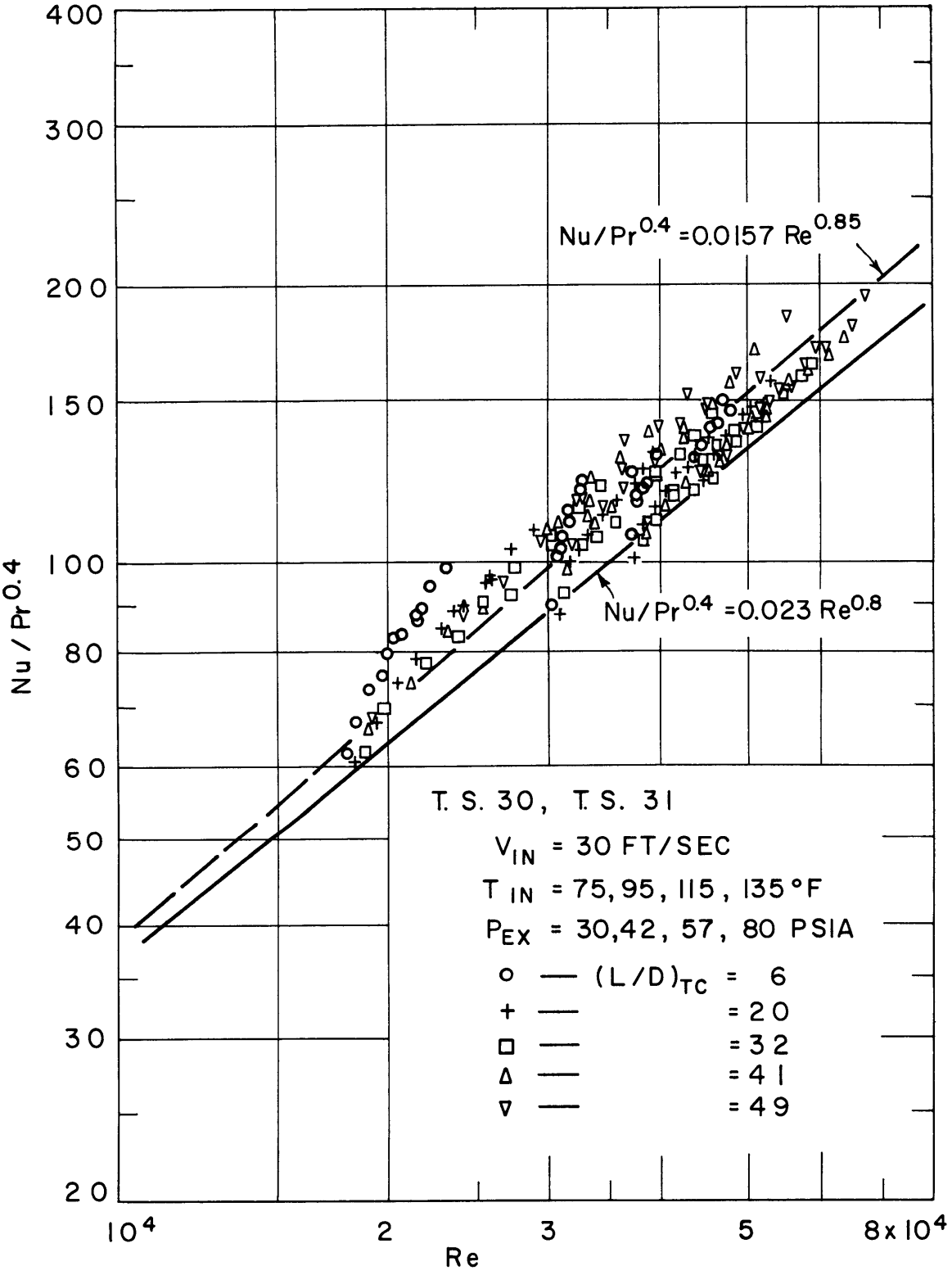

FIG. 4 CORRELATION OF NON-BOILING HEAT TRANSFER DATA

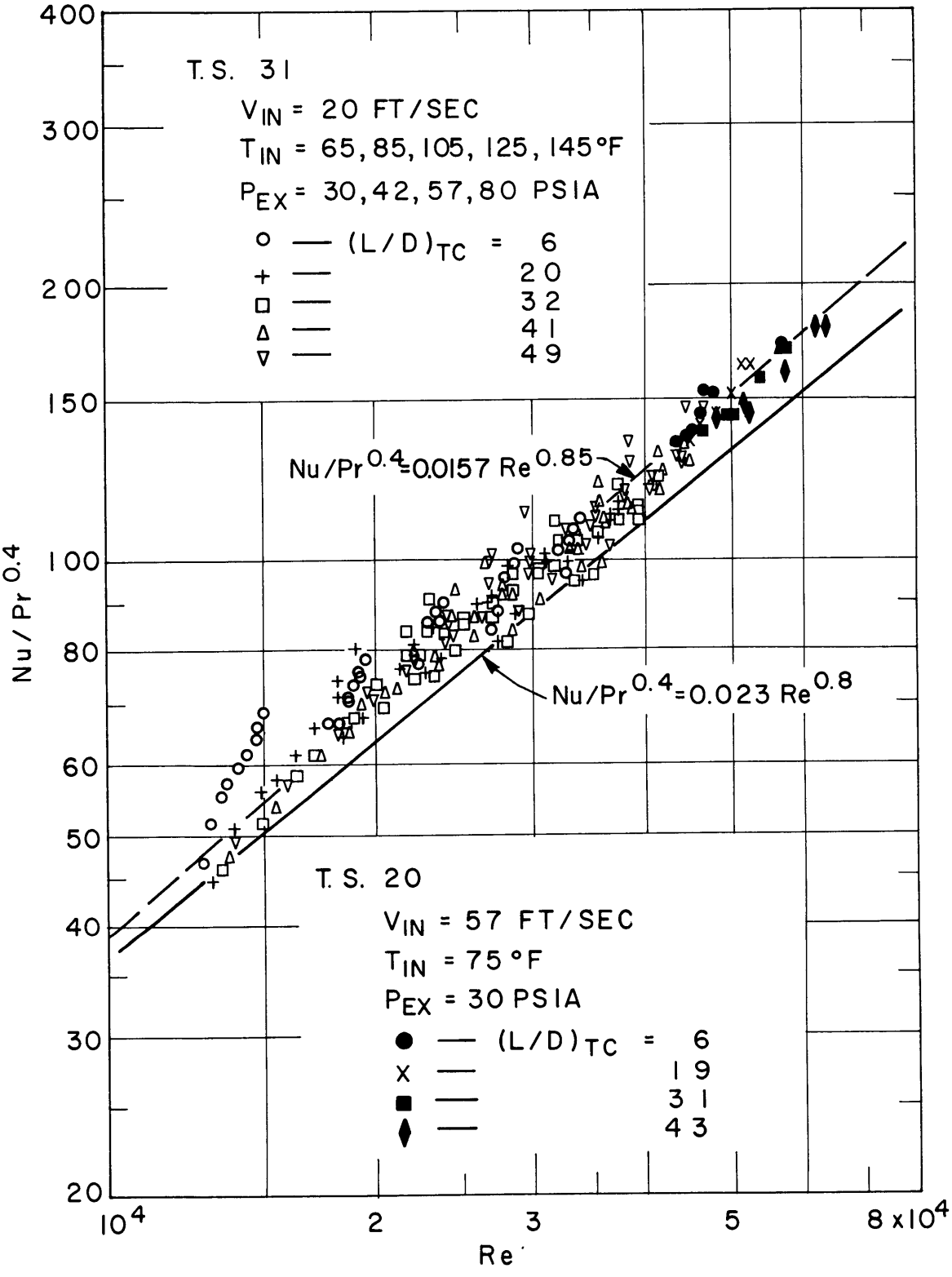

FIG. 5 CORRELATION OF NON-BOILING HEAT TRANSFER DATA

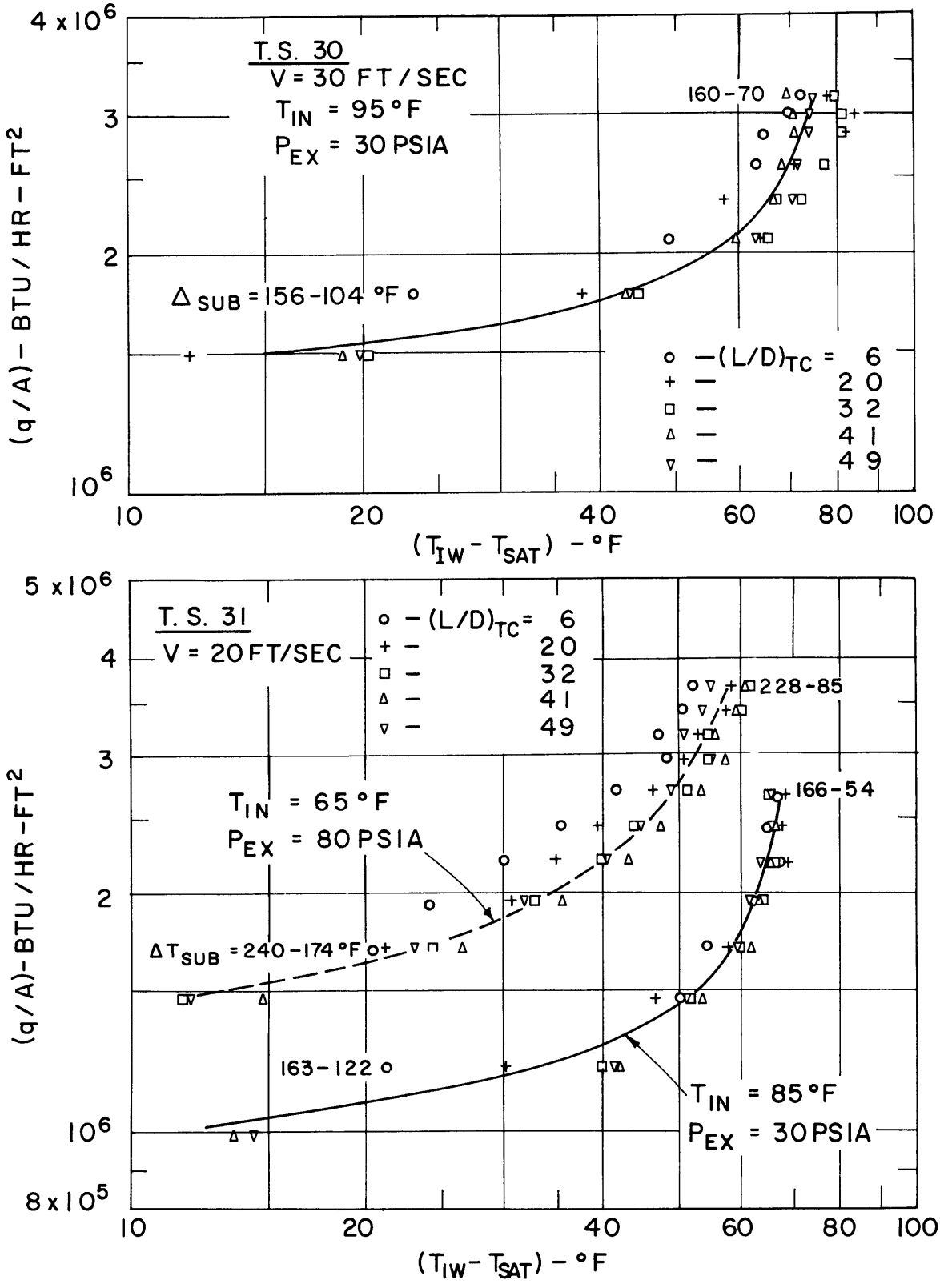

FIG. 6 BOILING CURVES - TYPICAL DATA

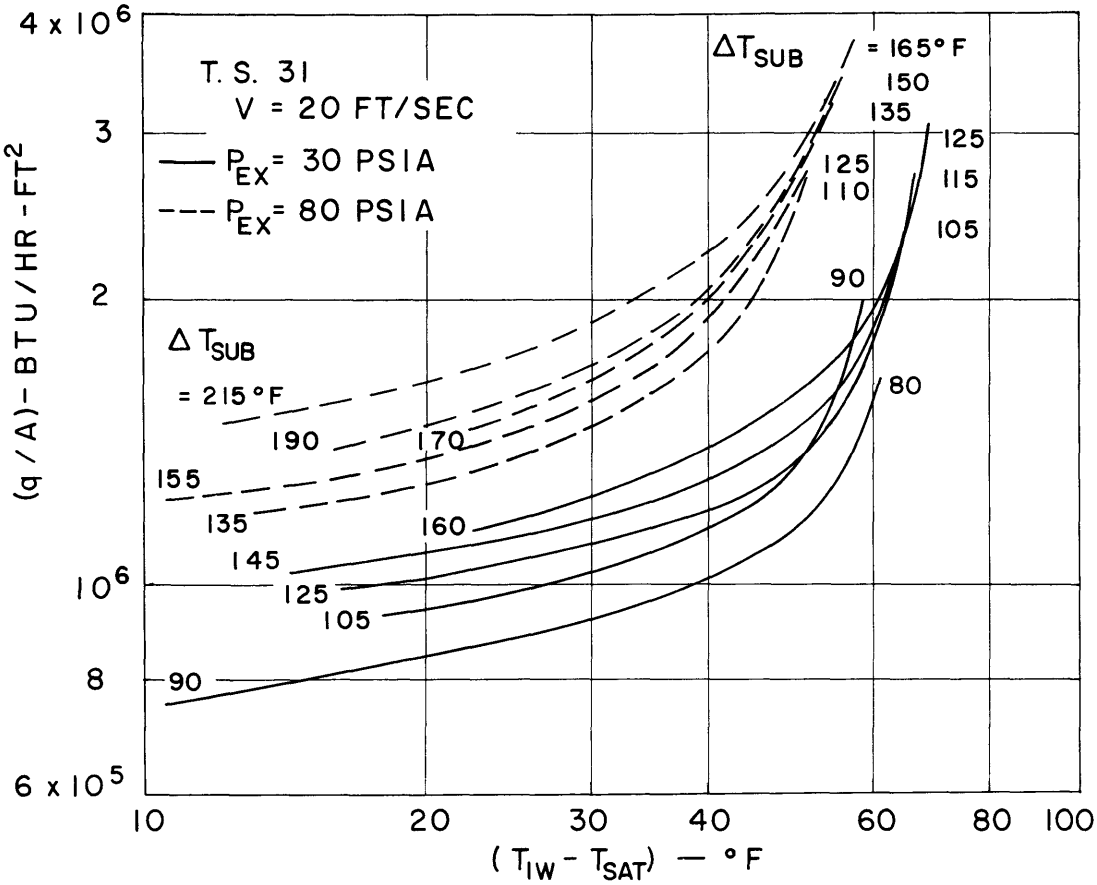

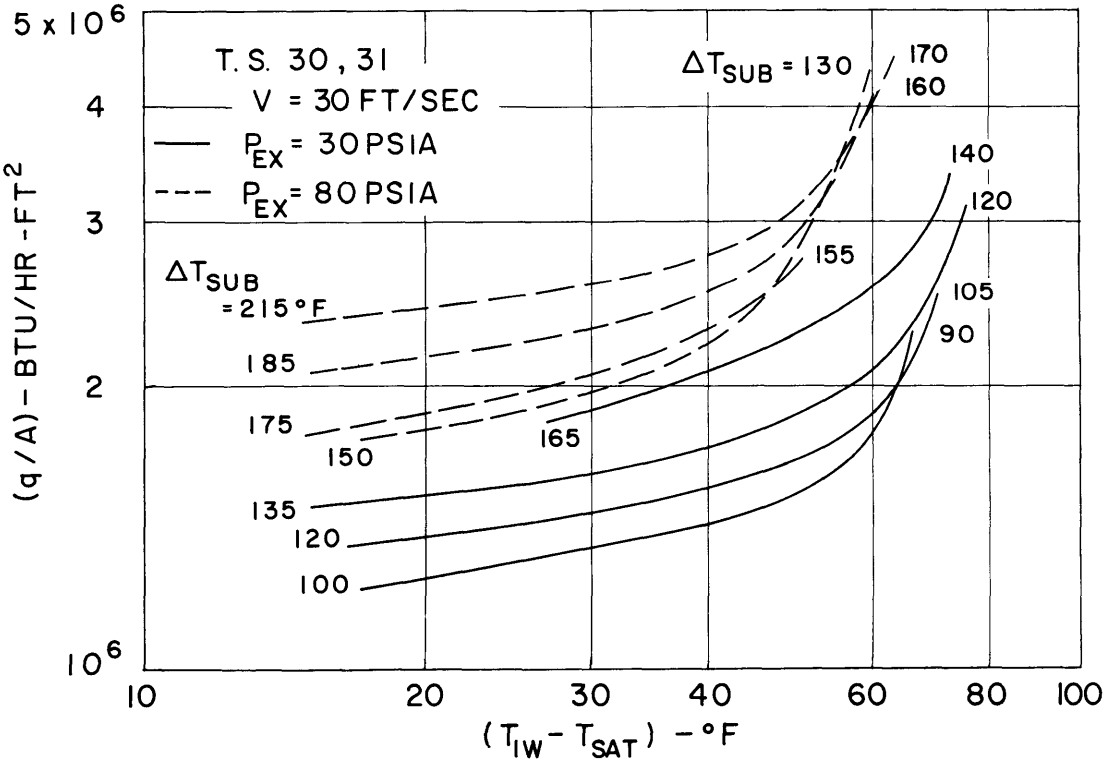

FIG. 7 BOILING CURVES - AVERAGE LINES

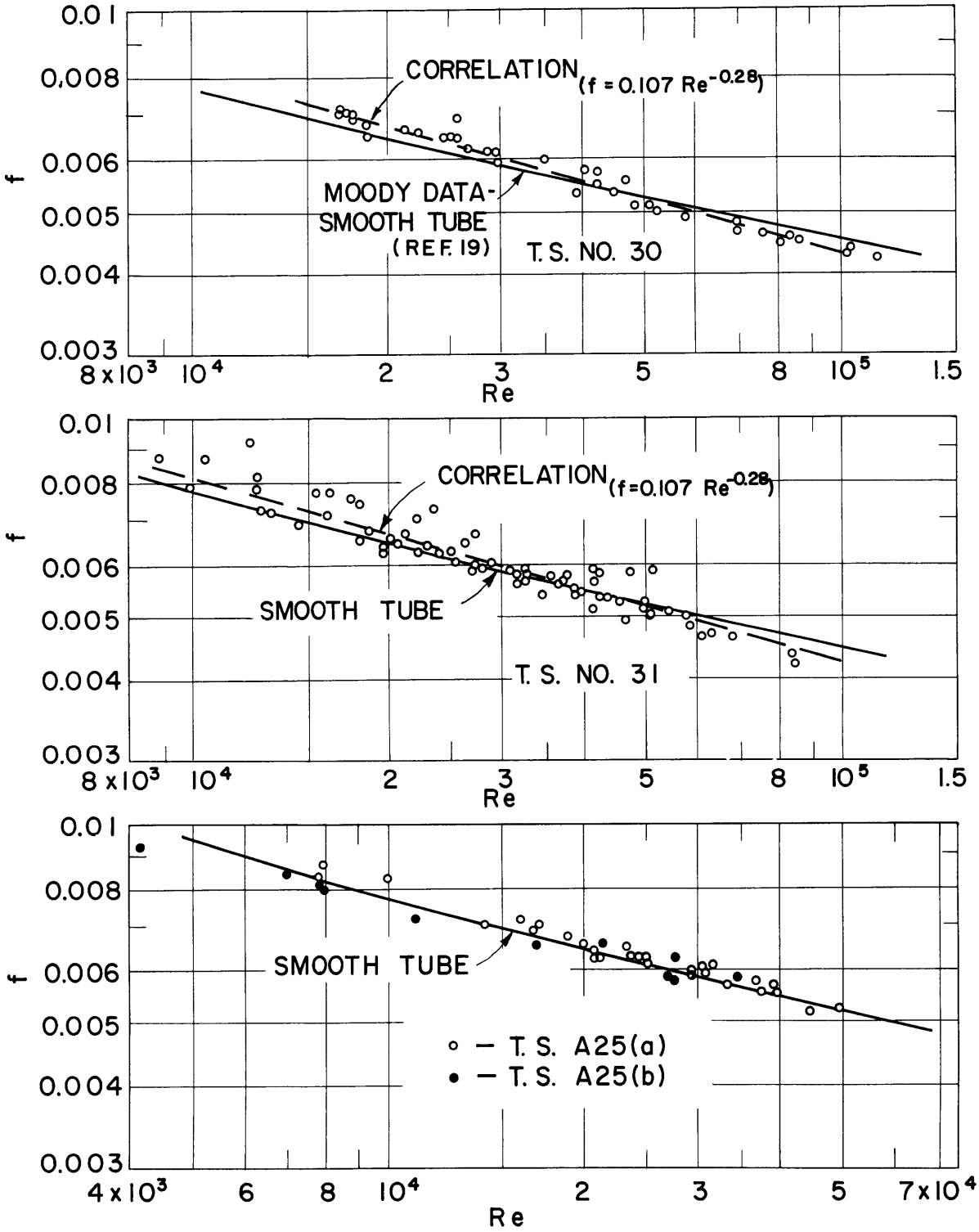

FIG. 8 ISOTHERMAL FRICTION FACTOR CORRELATION

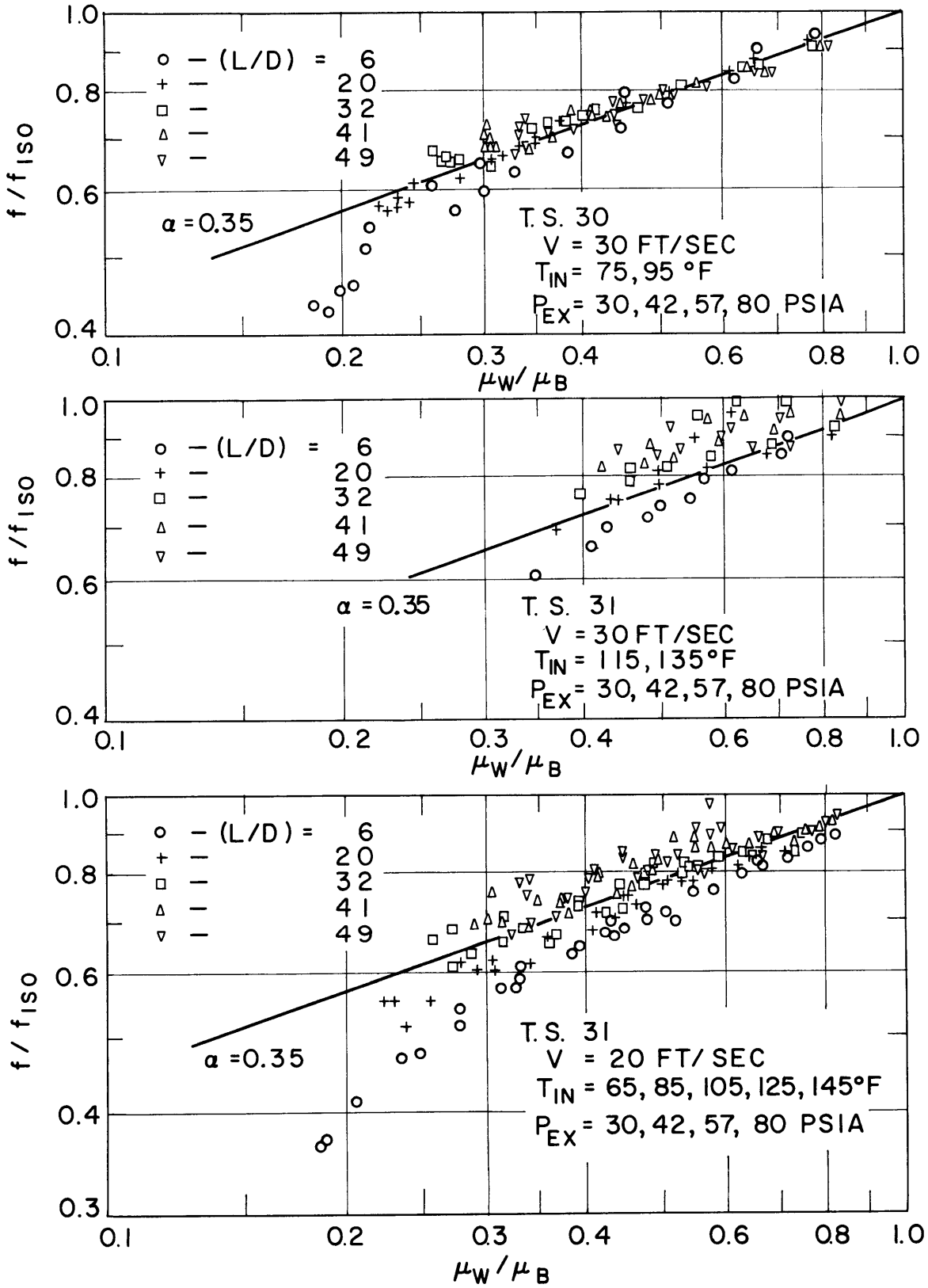

FIG. 9 CORRELATION OF NON-BOILING FRICTION FACTOR WITH VISCOSITY RATIO

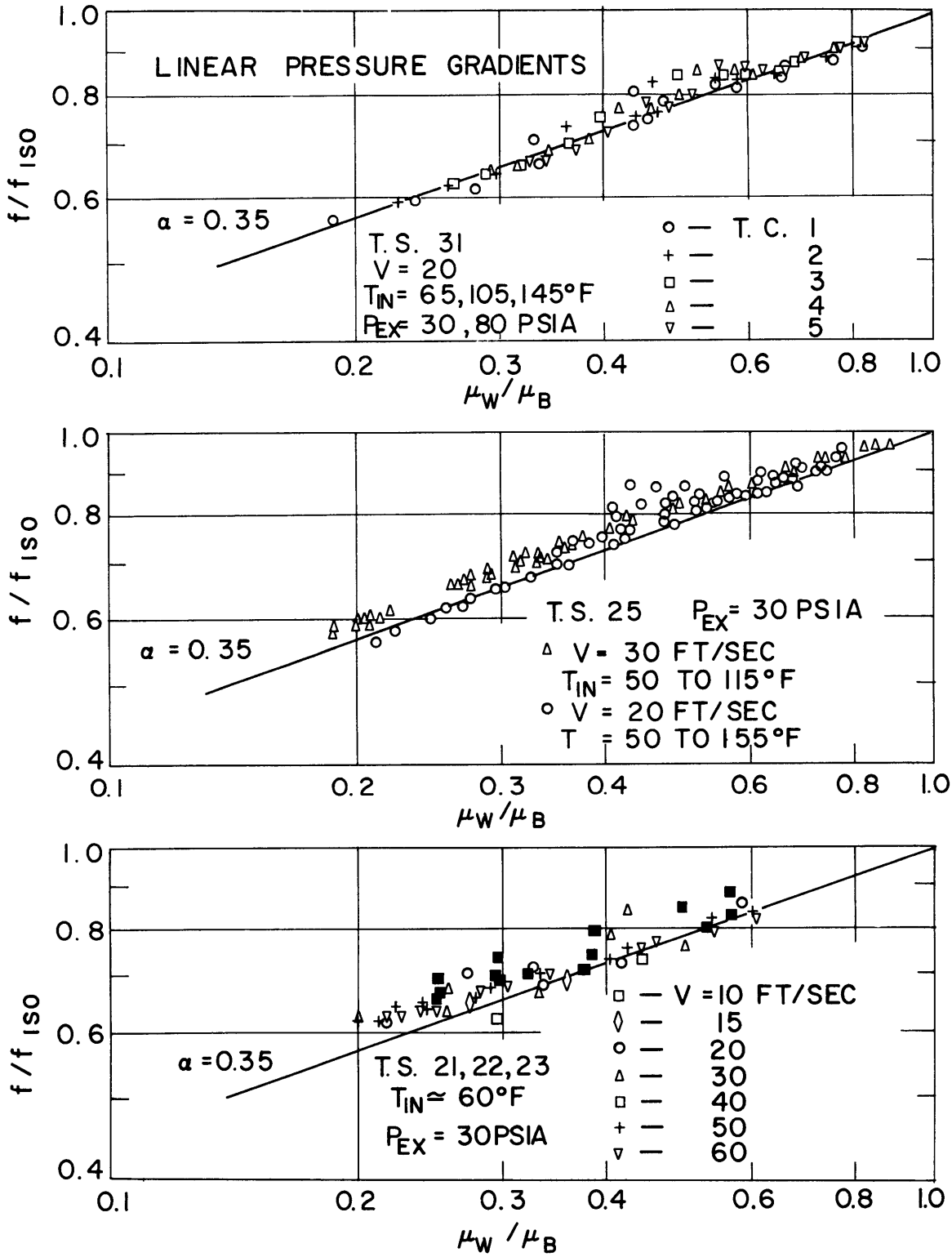

FIG. 10 CORRELATION OF NON-BOILING FRICTION FACTOR WITH VISCOSITY RATIO

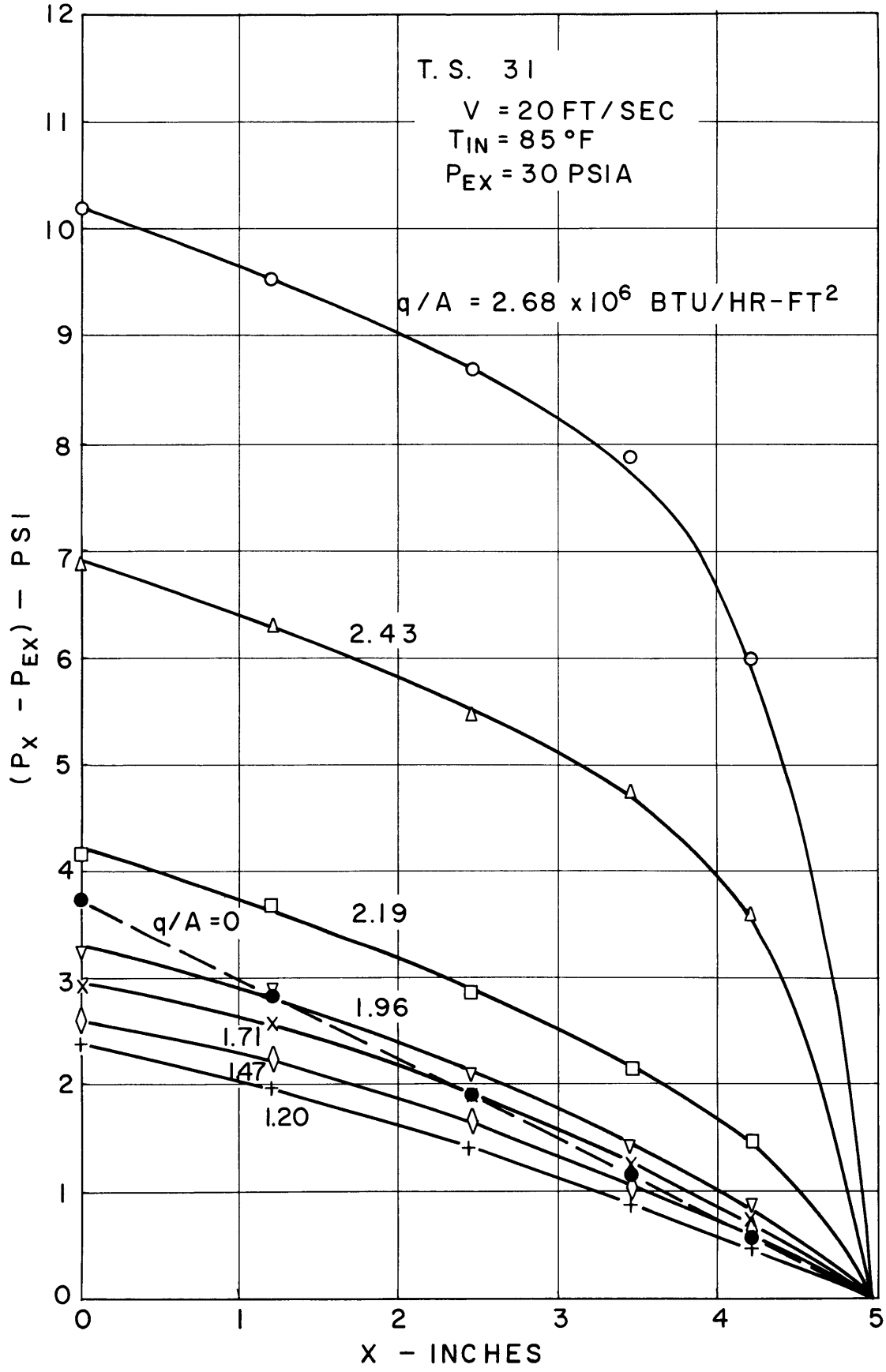

FIG. 11 PRESSURE DROP VS. DISTANCE

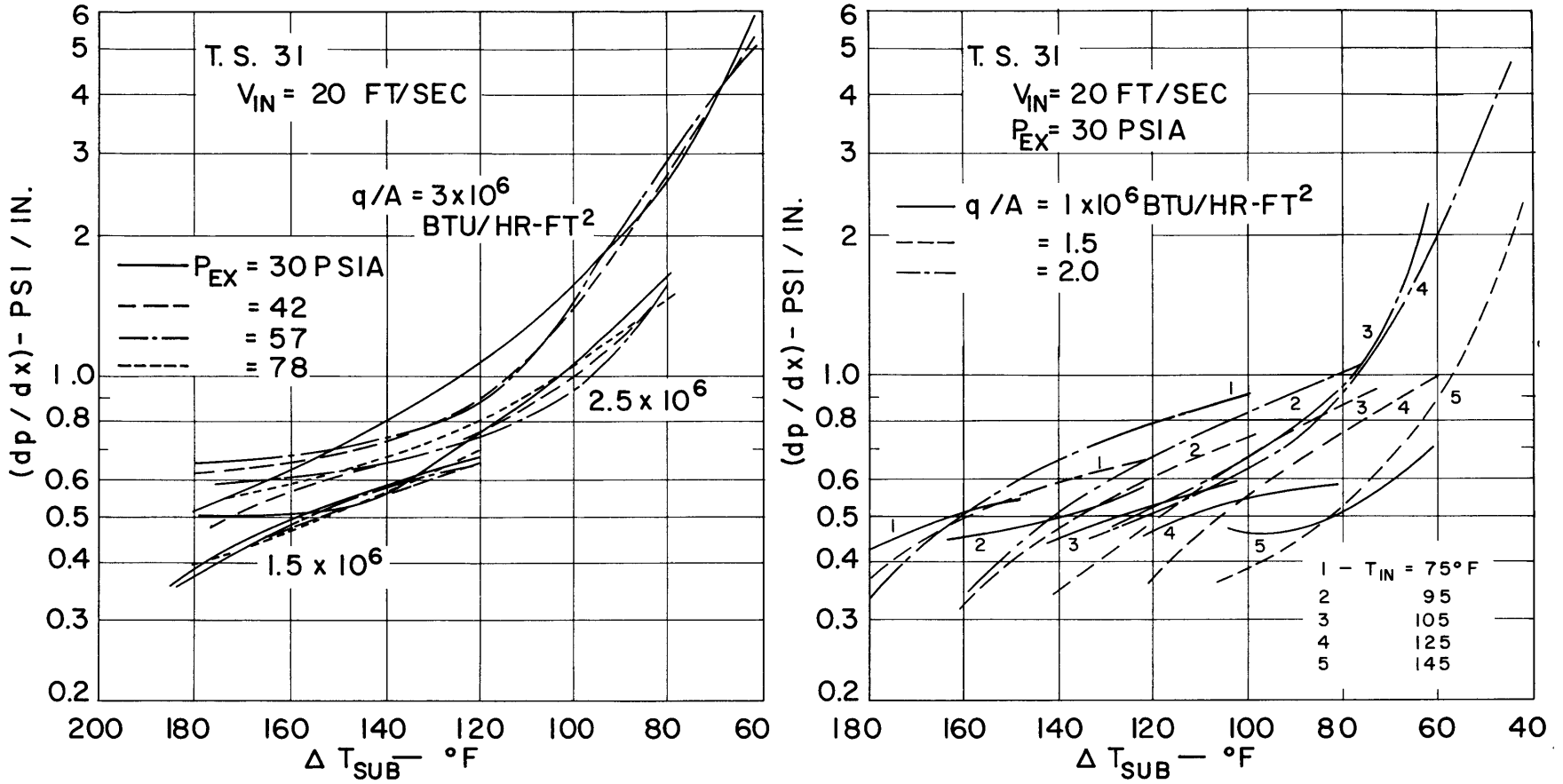

FIG. 12 PRESSURE GRADIENT VS. SUBCOOLING

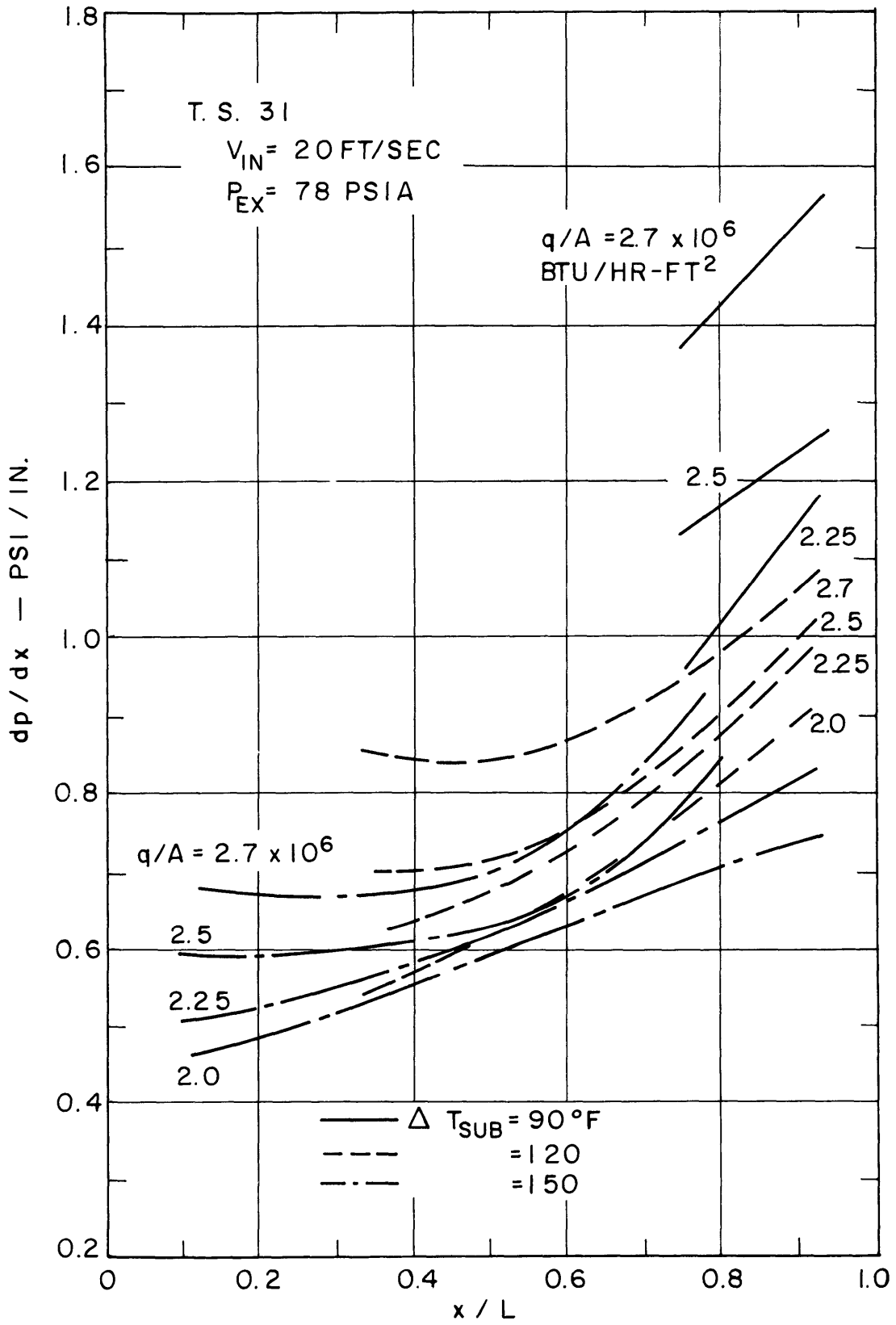

FIG. 13 PRESSURE GRADIENT VS. POSITION

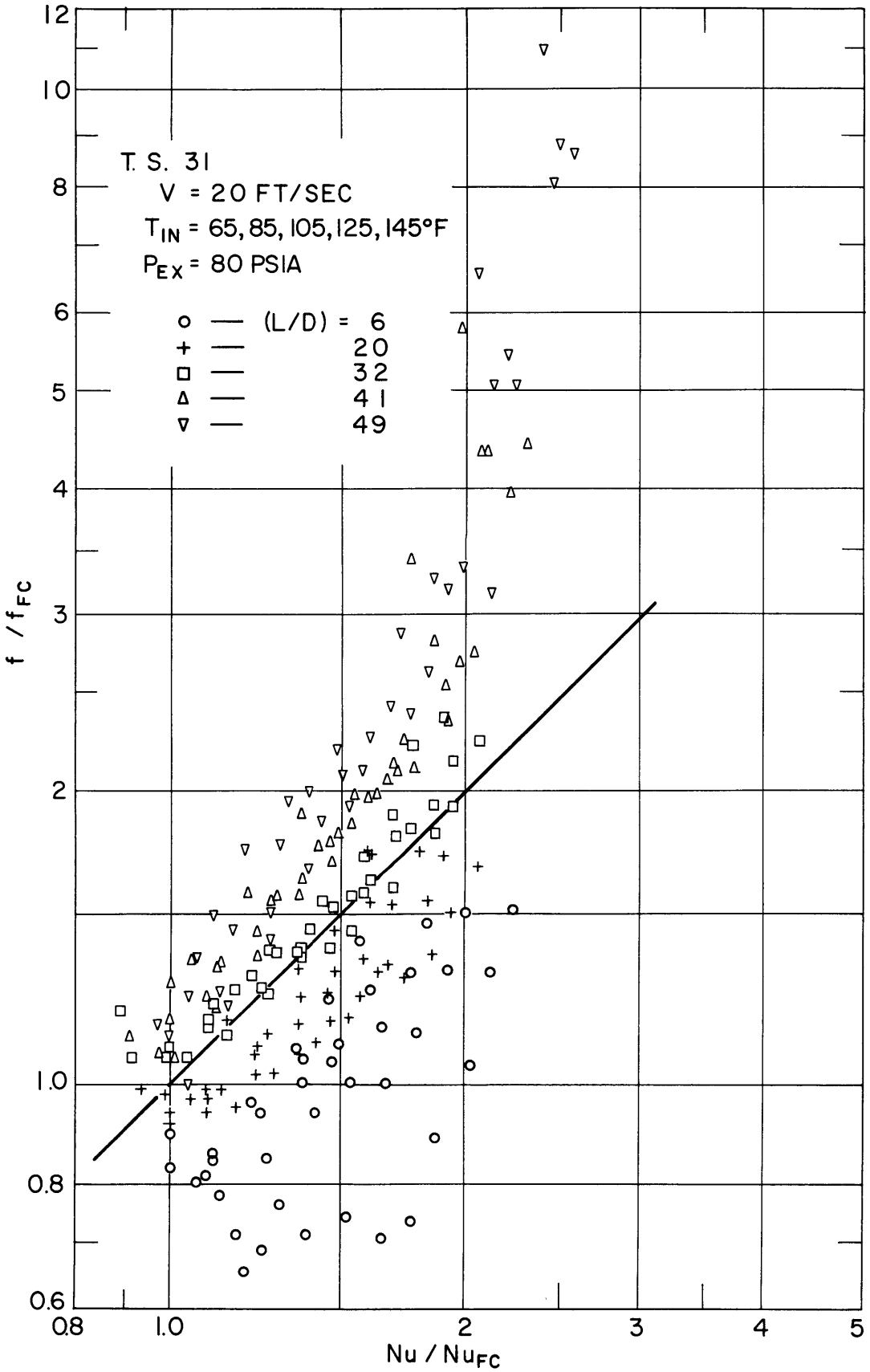

FIG. 14 HEAT TRANSFER - PRESSURE DROP ANALOGY

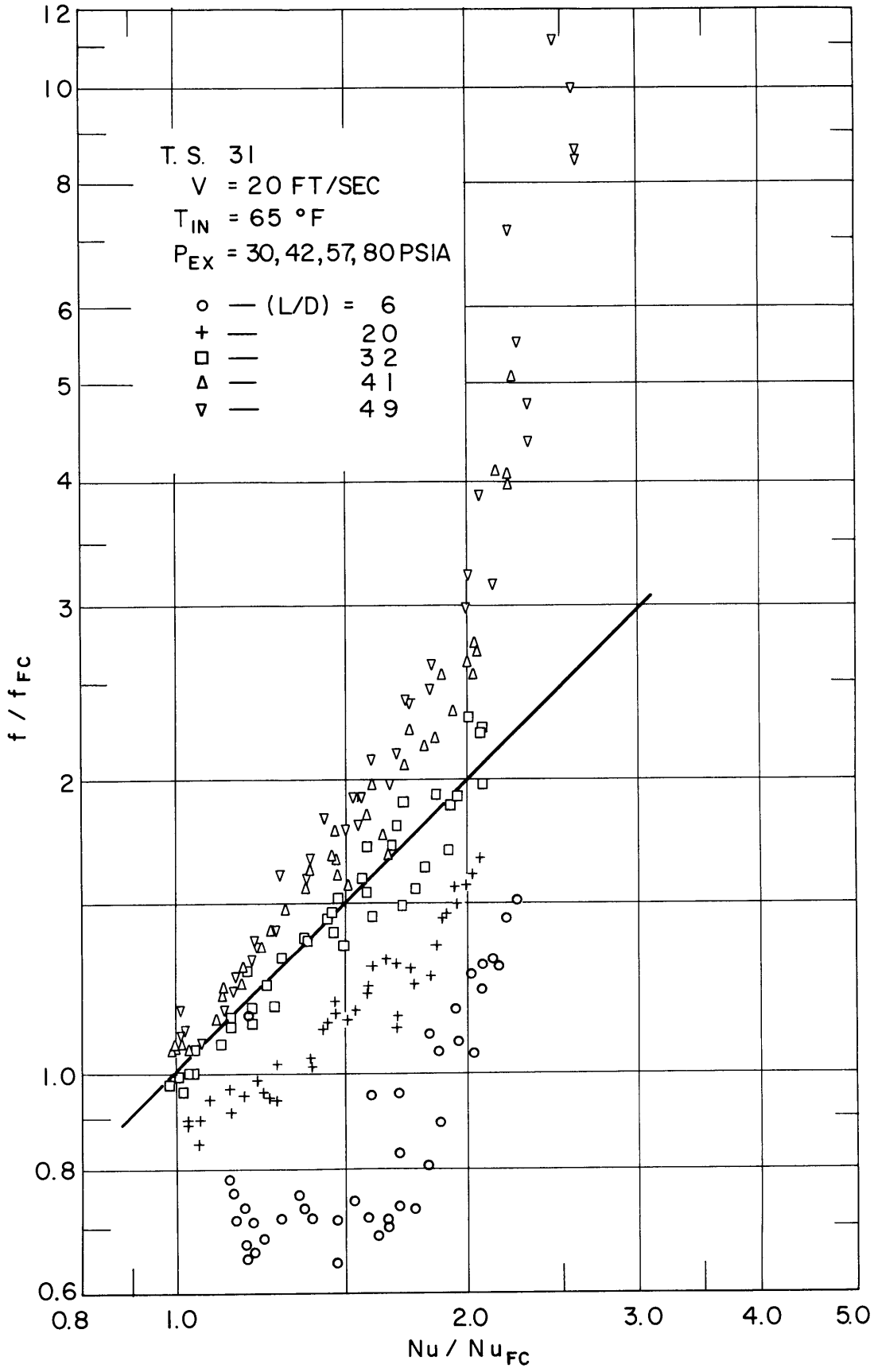

FIG. 15 HEAT TRANSFER - PRESSURE DROP ANALOGY

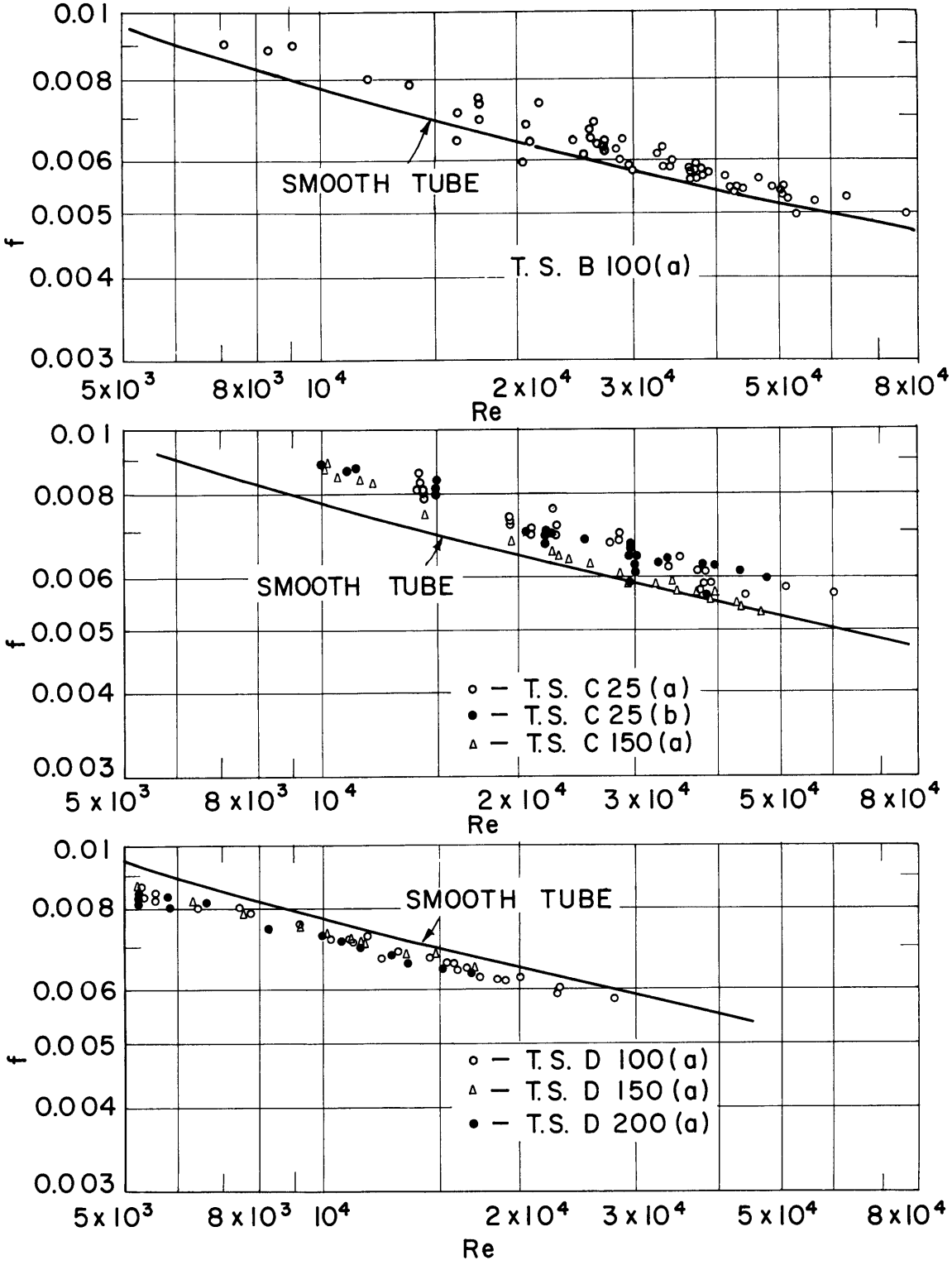

FIG. 16 ISOTHERMAL FRICTION FACTOR CORRELATION

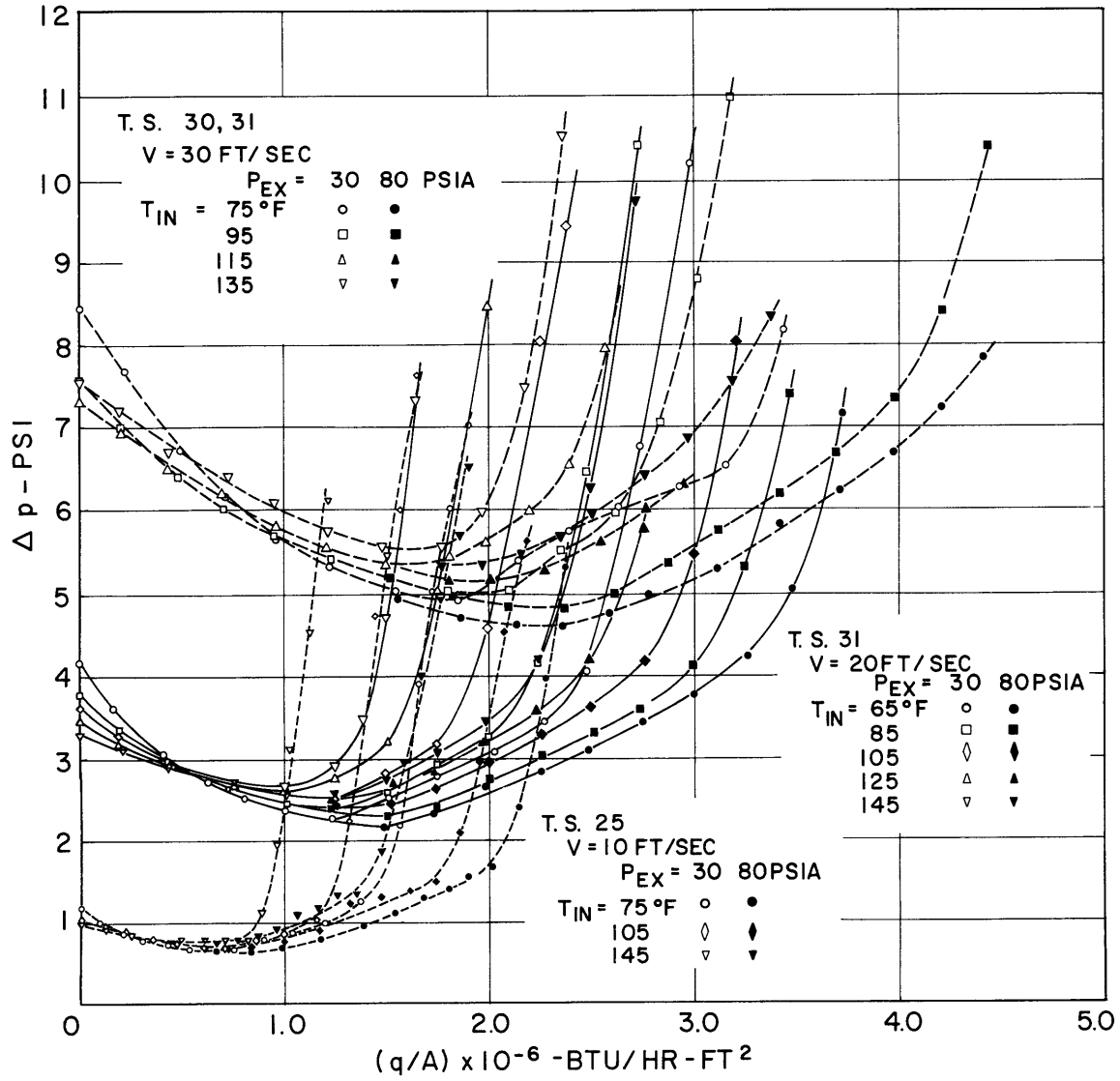

FIG. 17 PRESSURE DROP VS. HEAT FLUX - T. S.'s A50 VELOCITY, INLET TEMPERATURE, EXIT PRESSURE AS PARAMETERS

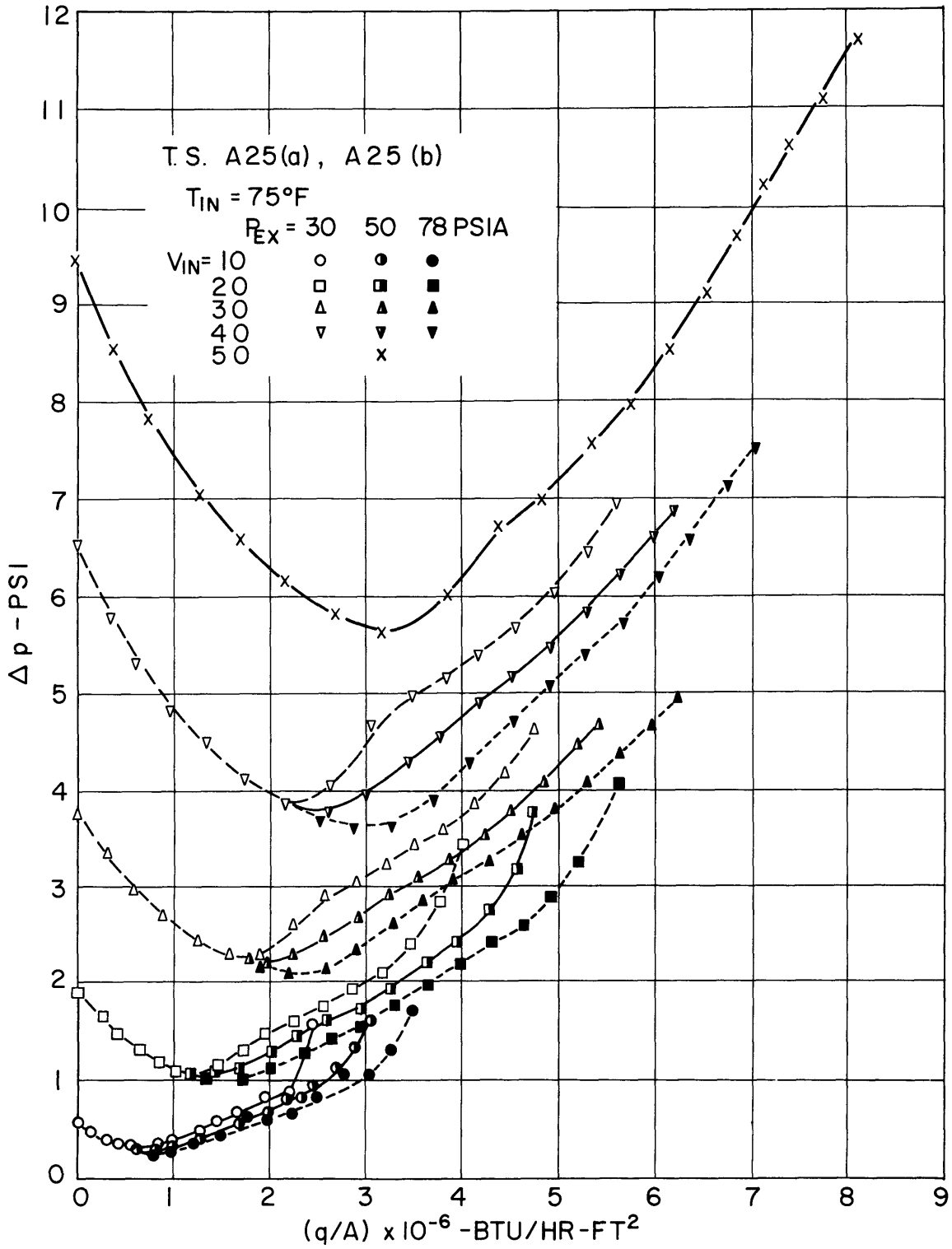

FIG. 18 PRESSURE DROP VS. HEAT FLUX - T. S.'s A25
VELOCITY AND EXIT PRESSURE AS PARAMETERS

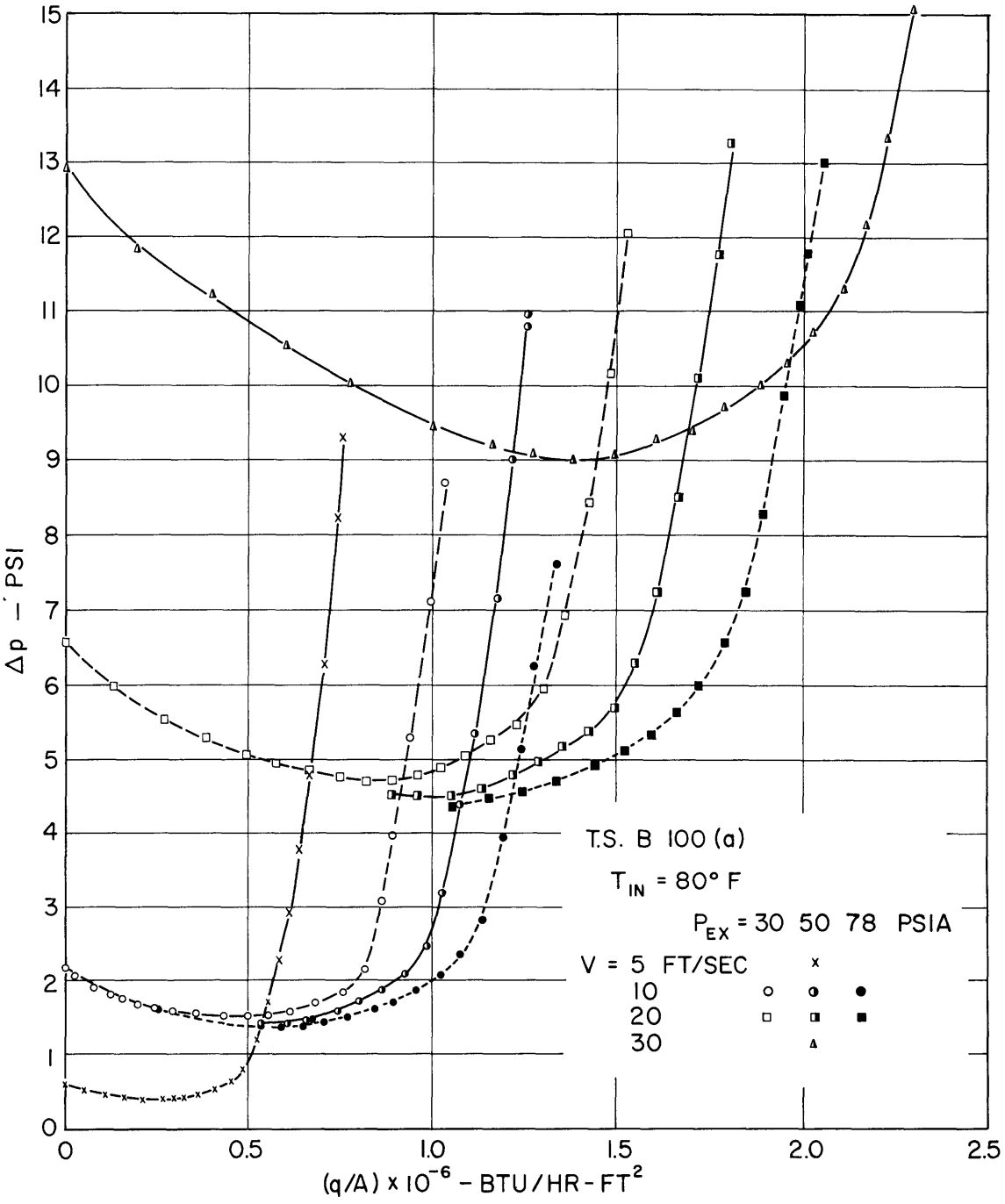

FIG. 19 PRESSURE DROP VS HEAT FLUX – T. S. B 100
VELOCITY AND EXIT PRESSURE AS PARAMETERS

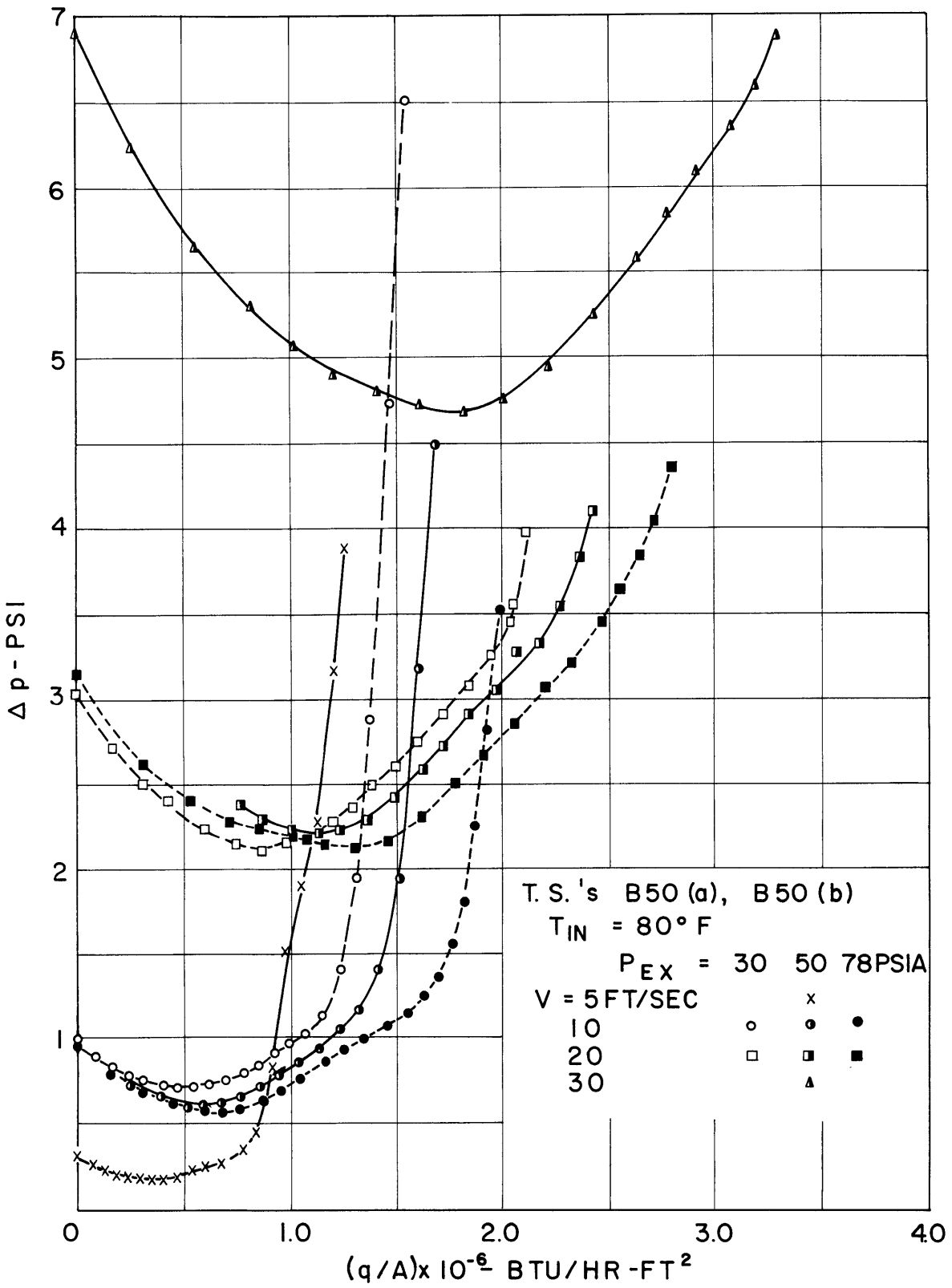

FIG. 20 PRESSURE DROP VS HEAT FLUX - T. S. B 50
VELOCITY AND PRESSURE AS PARAMETERS

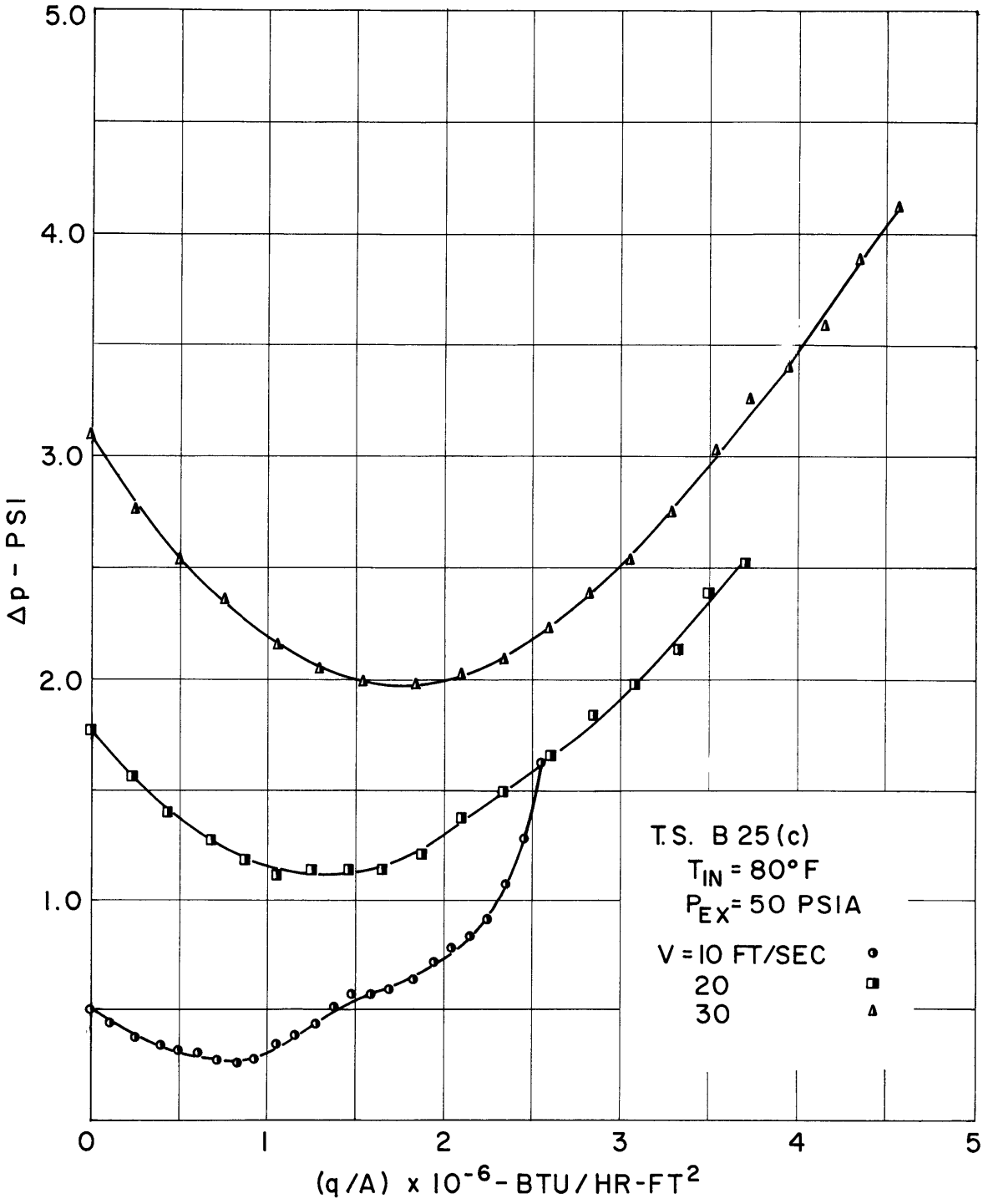

FIG. 21 PRESSURE DROP VS. HEAT FLUX - T. S. B25
VELOCITY AS A PARAMETER

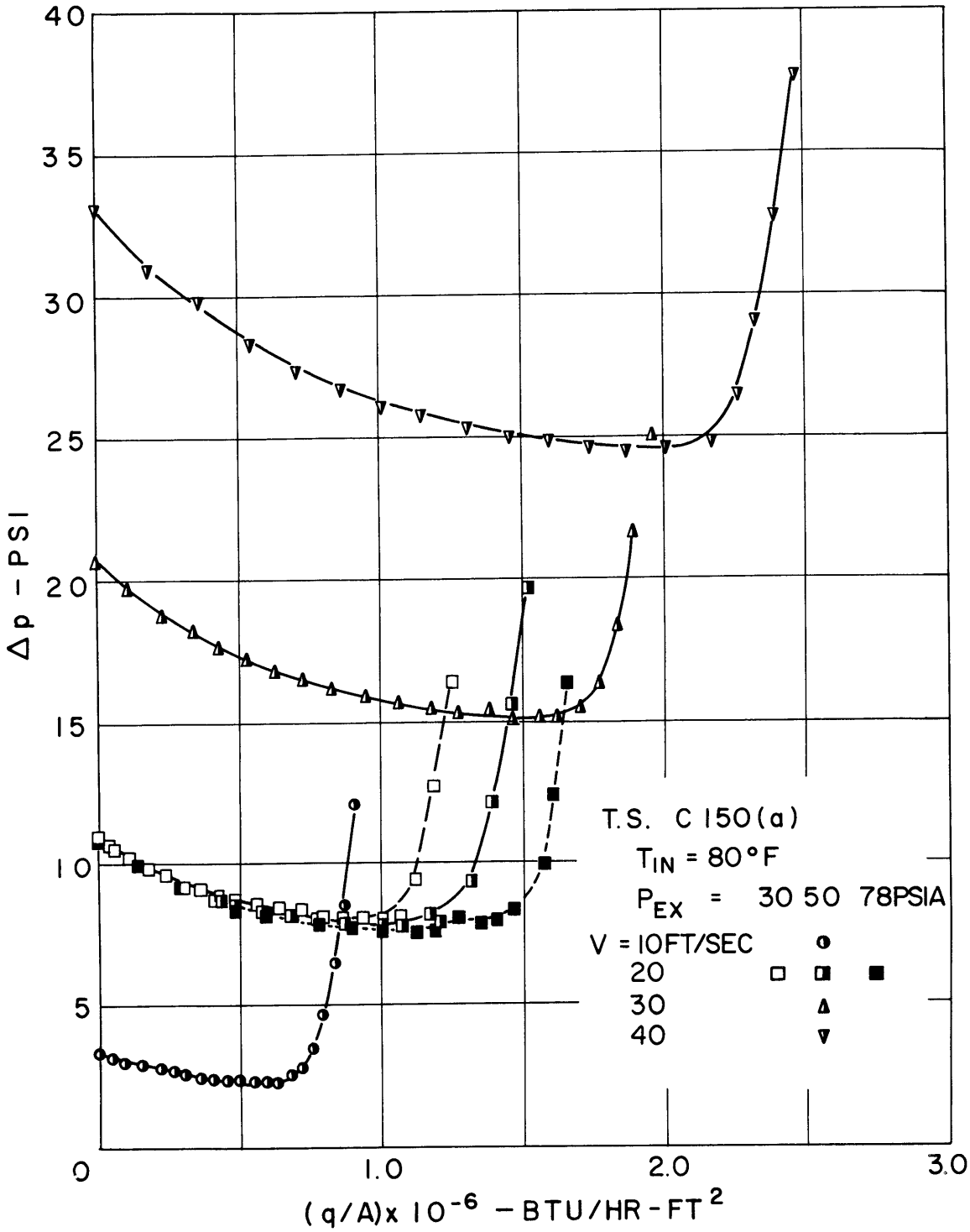

FIG. 22 PRESSURE DROP VS. HEAT FLUX - T.S. C 150
VELOCITY AND PRESSURE AS PARAMETERS

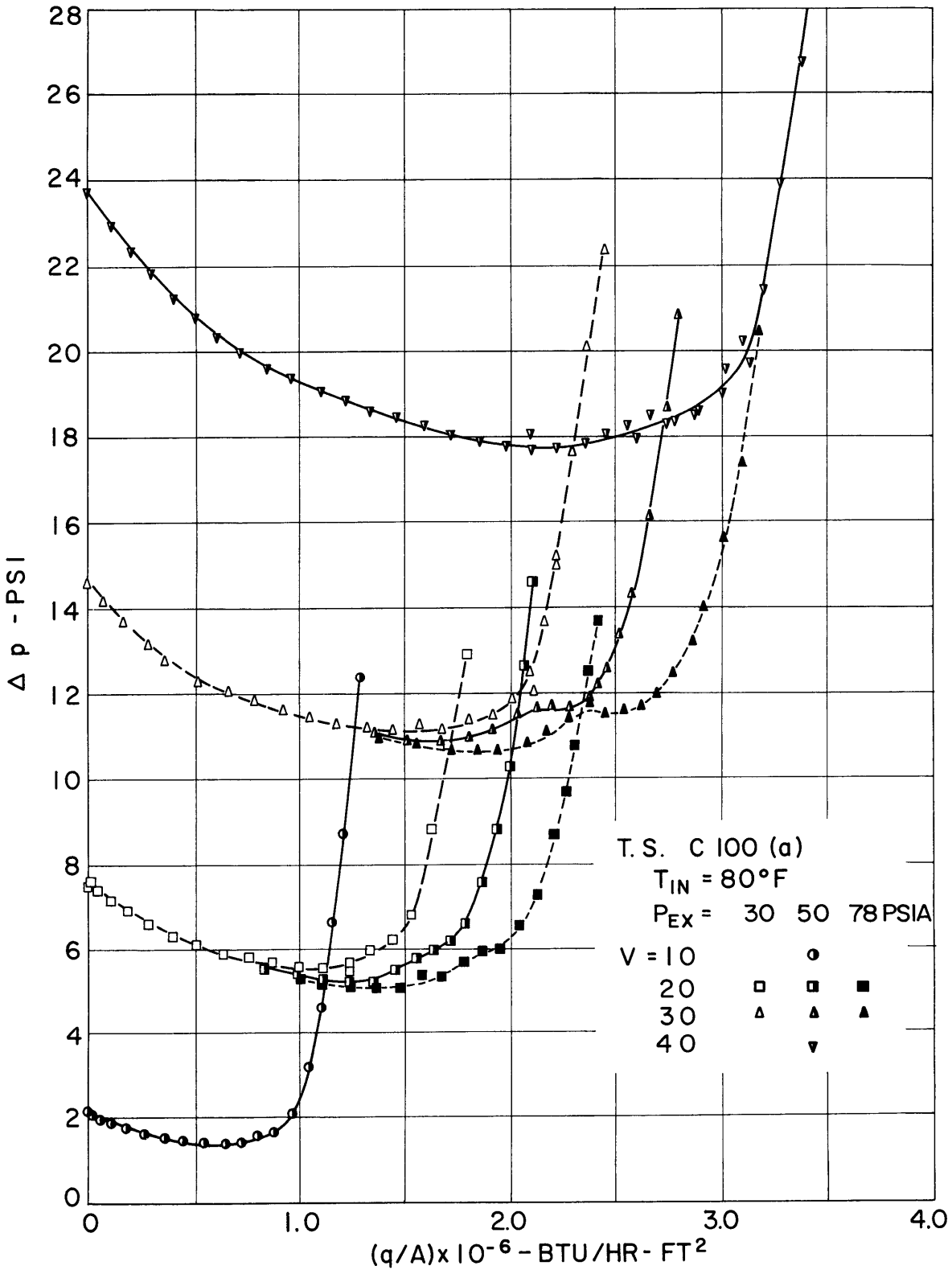

FIG. 23 PRESSURE DROP VS. HEAT FLUX - T.S. C100
VELOCITY AND PRESSURE AS PARAMETERS

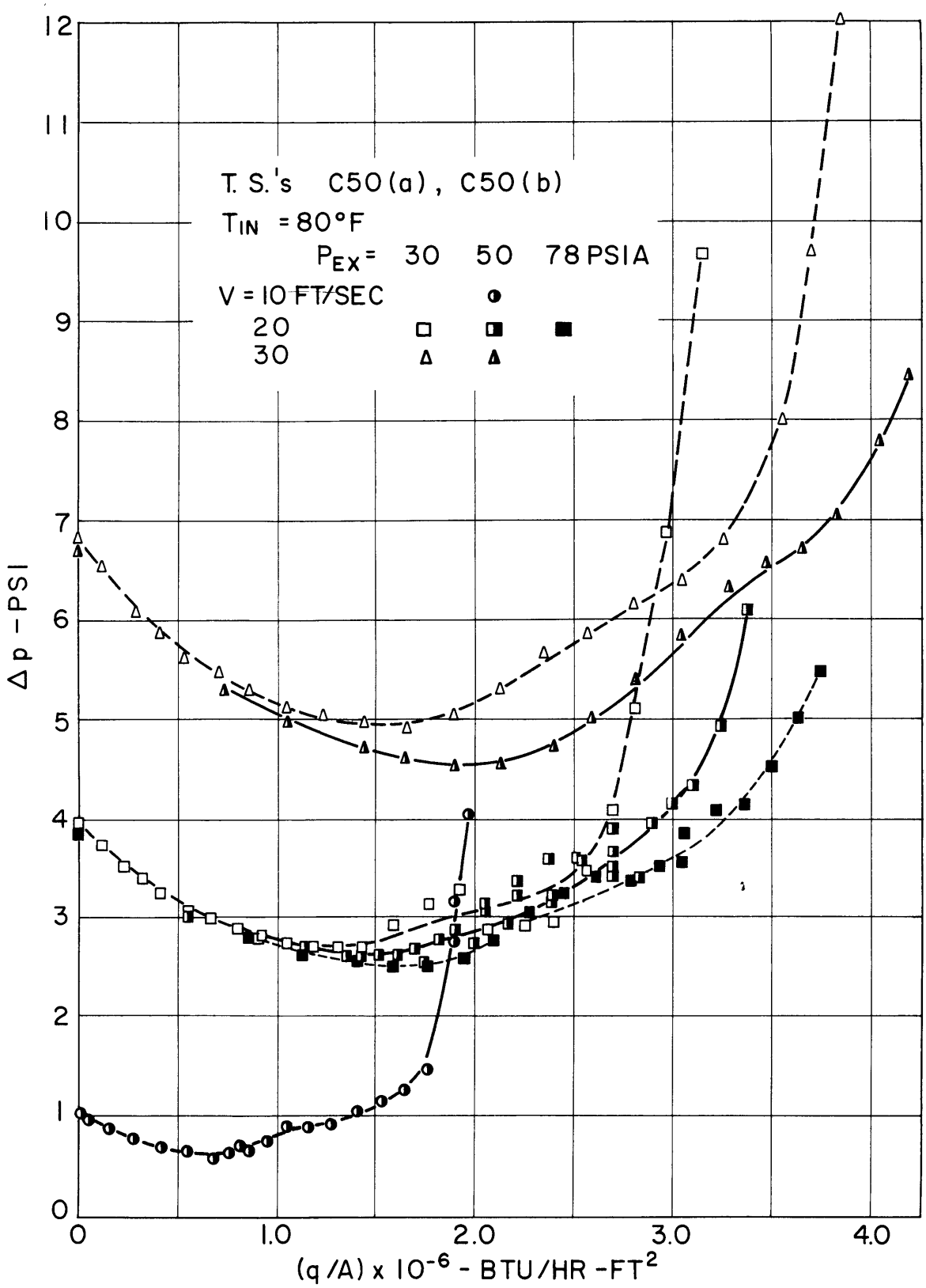

FIG. 24 PRESSURE DROP VS. HEAT FLUX - T. S. C50
VELOCITY AND PRESSURE AS PARAMETERS

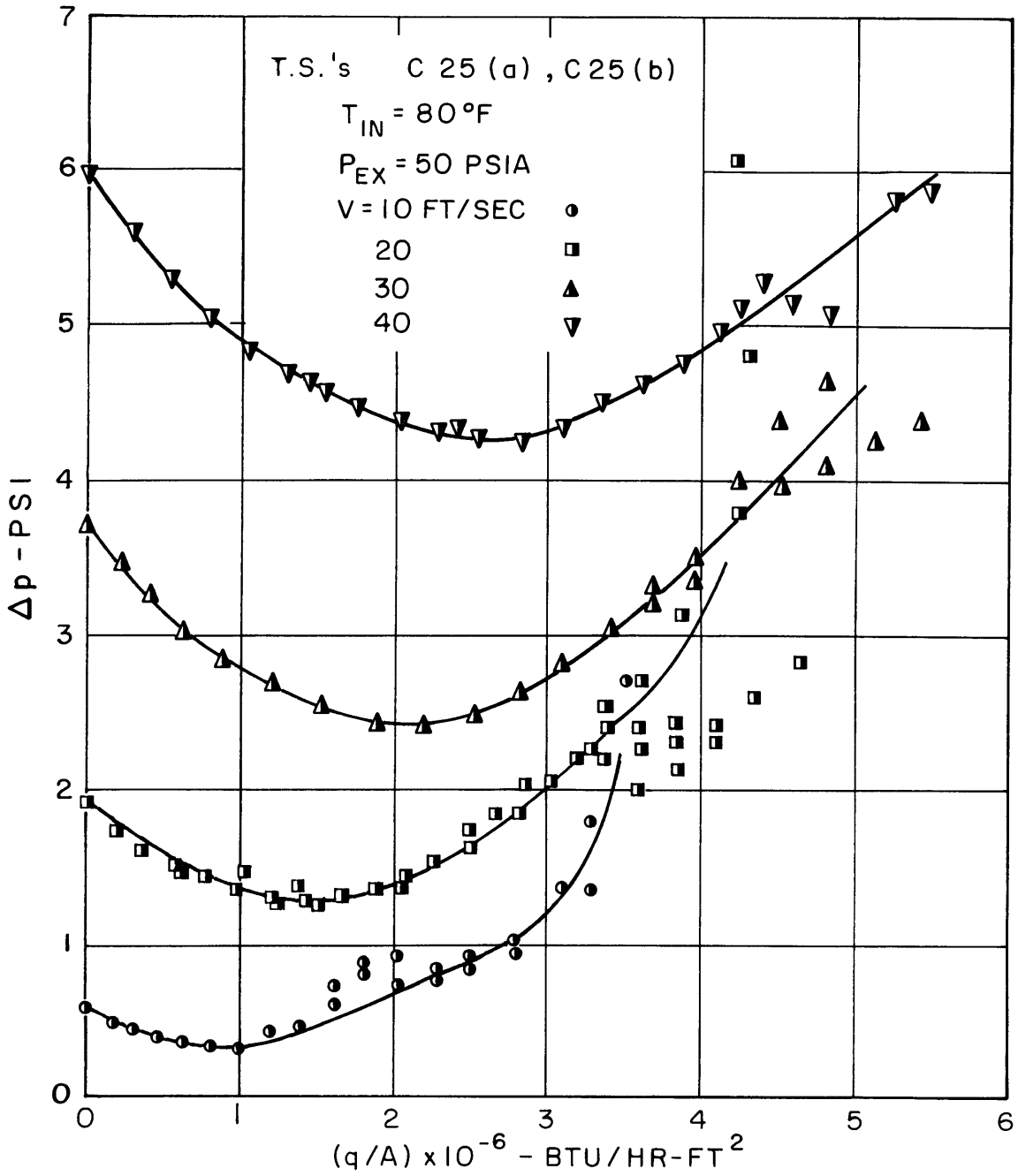

FIG. 25 PRESSURE DROP VS. HEAT FLUX - T. S. C25
VELOCITY AS A PARAMETER

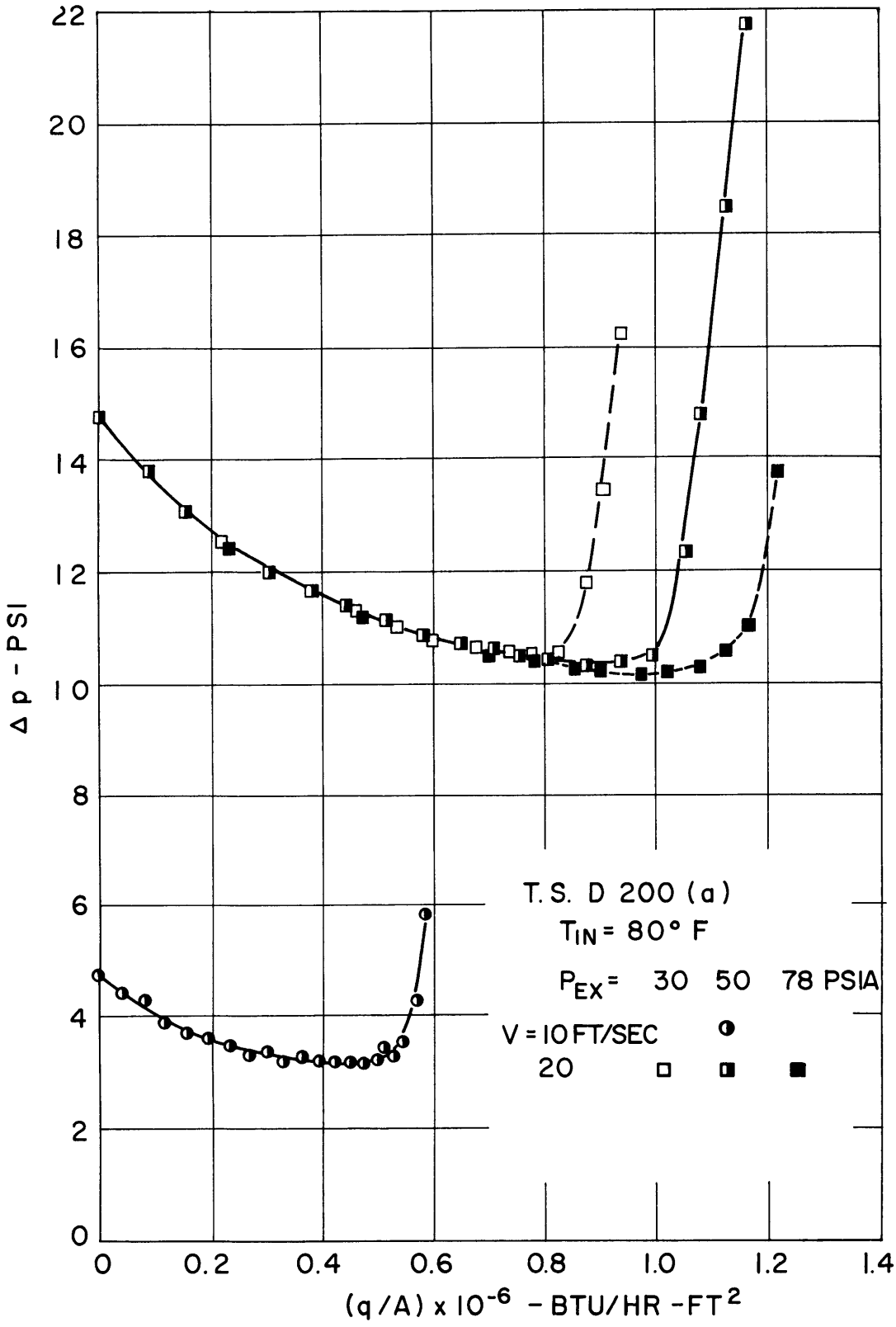

FIG. 26 PRESSURE DROP VS. HEAT FLUX - T. S. D200
VELOCITY AND PRESSURE AS PARAMETERS

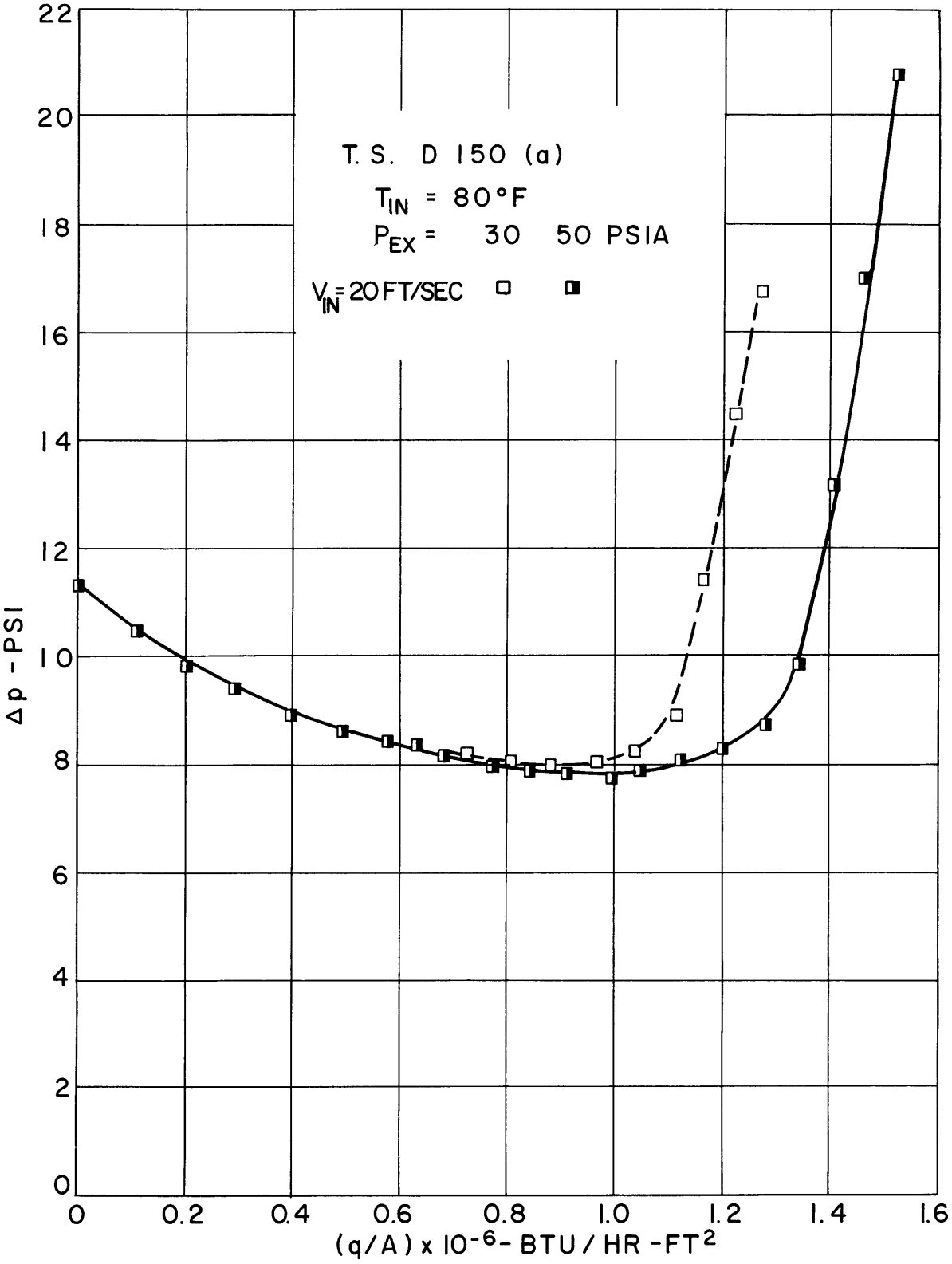

FIG. 27 PRESSURE DROP VS. HEAT FLUX - T. S. D150
PRESSURE AS A PARAMETER

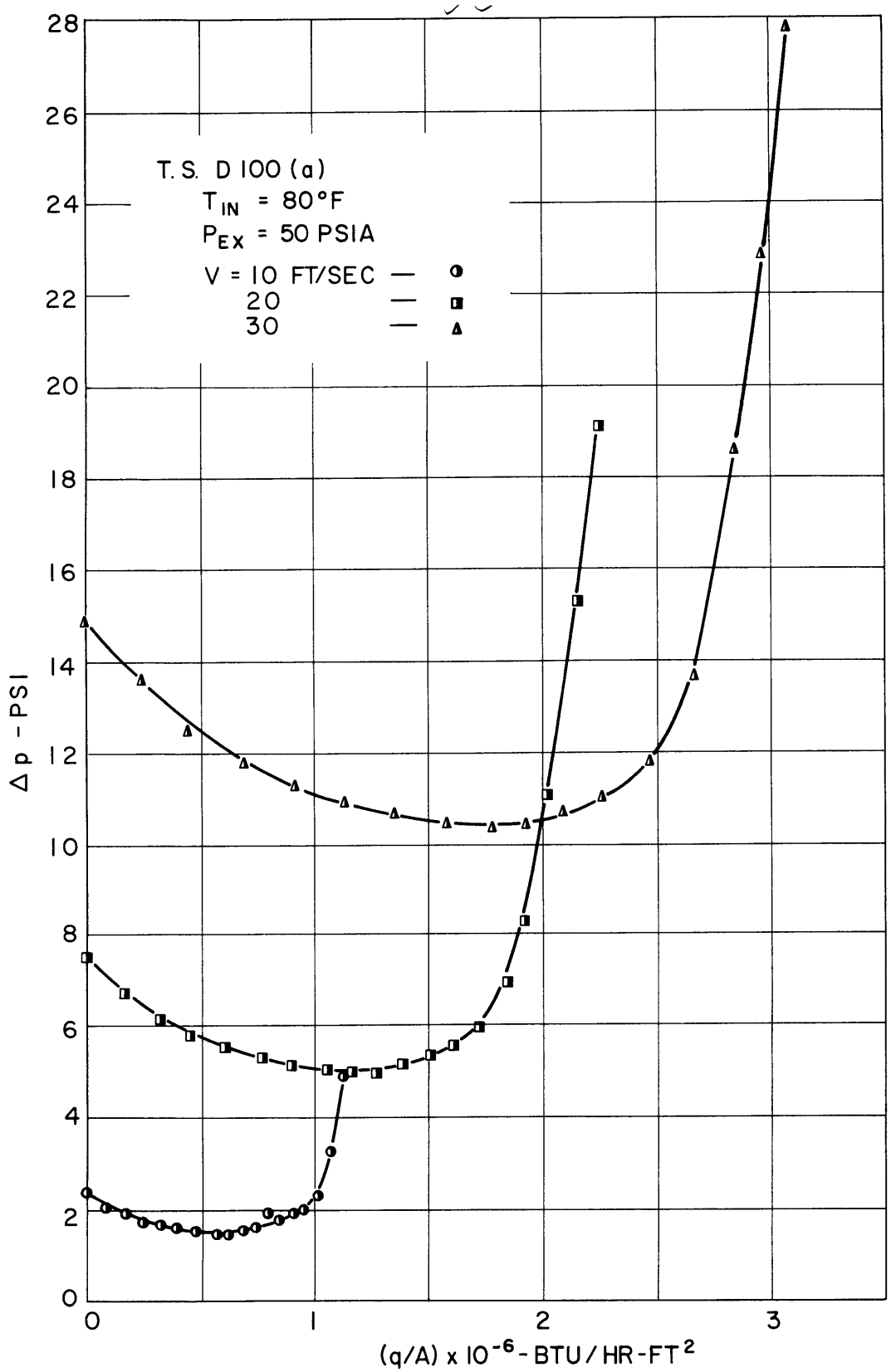

FIG. 28 PRESSURE DROP VS. HEAT FLUX - T. S. D100
VELOCITY AS A PARAMETER

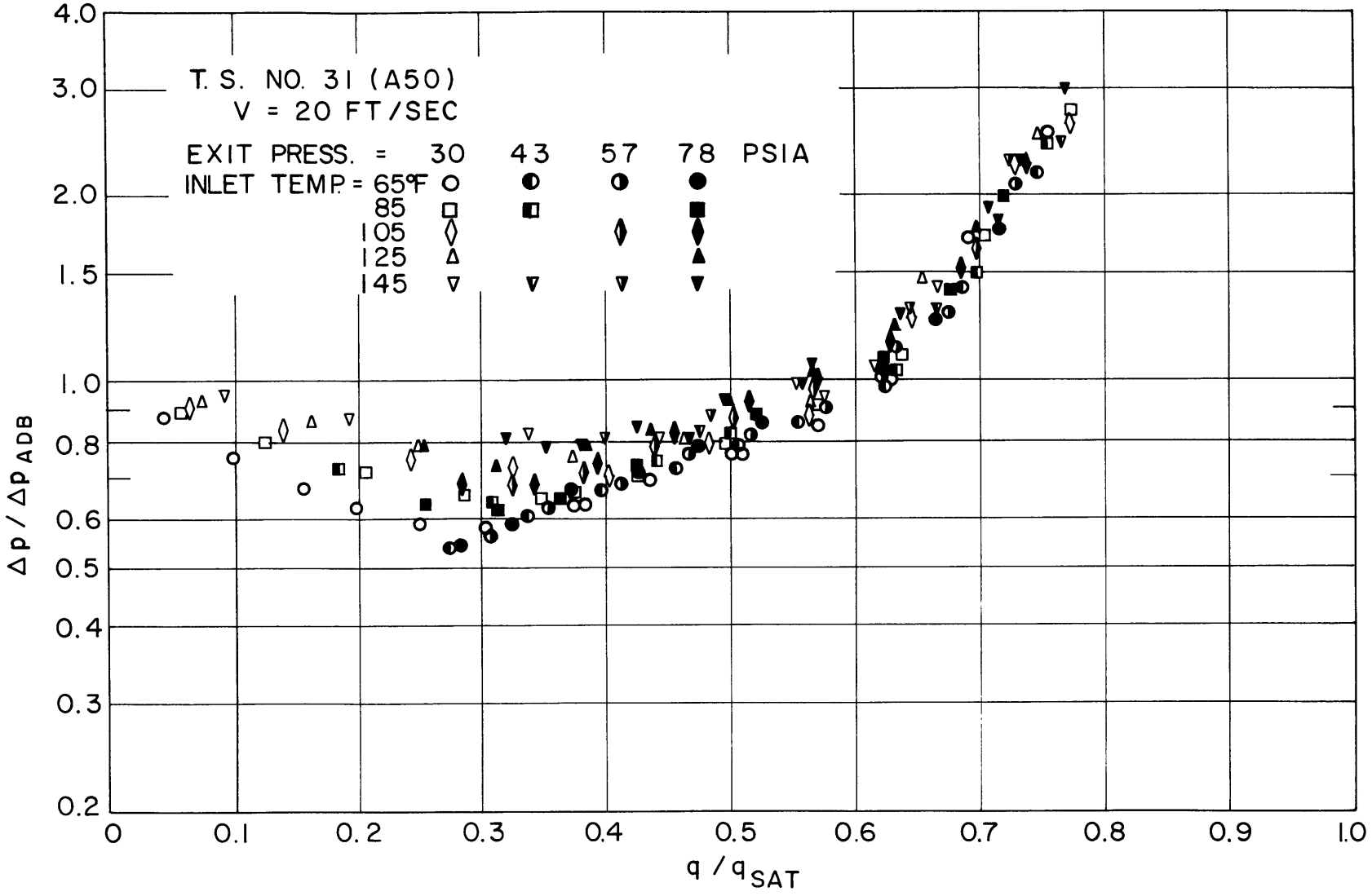

FIG. 29 CORRELATED PRESSURE DROP DATA – T. S. A50

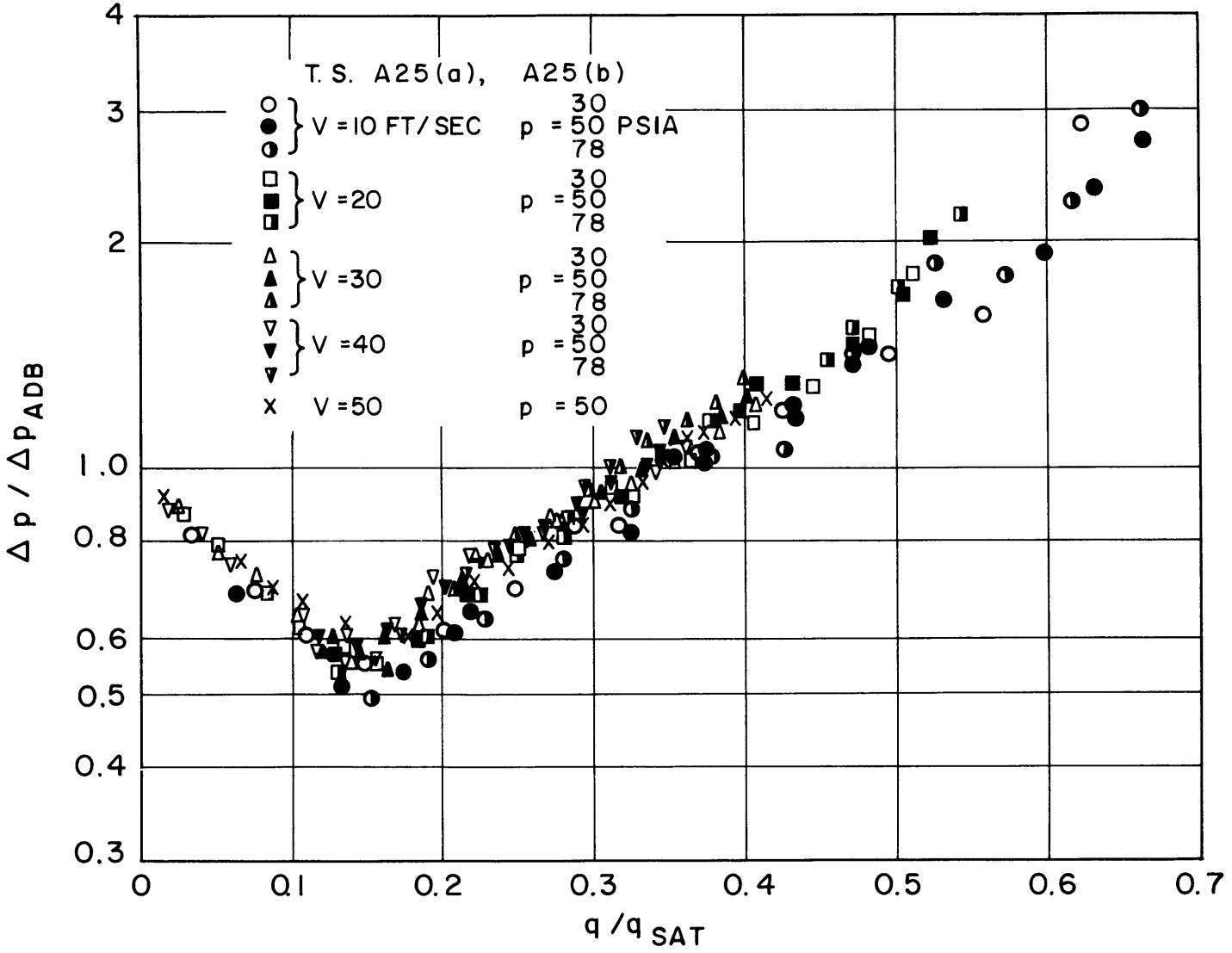

FIG. 30 CORRELATED PRESSURE DROP DATA – T.S.'s A25

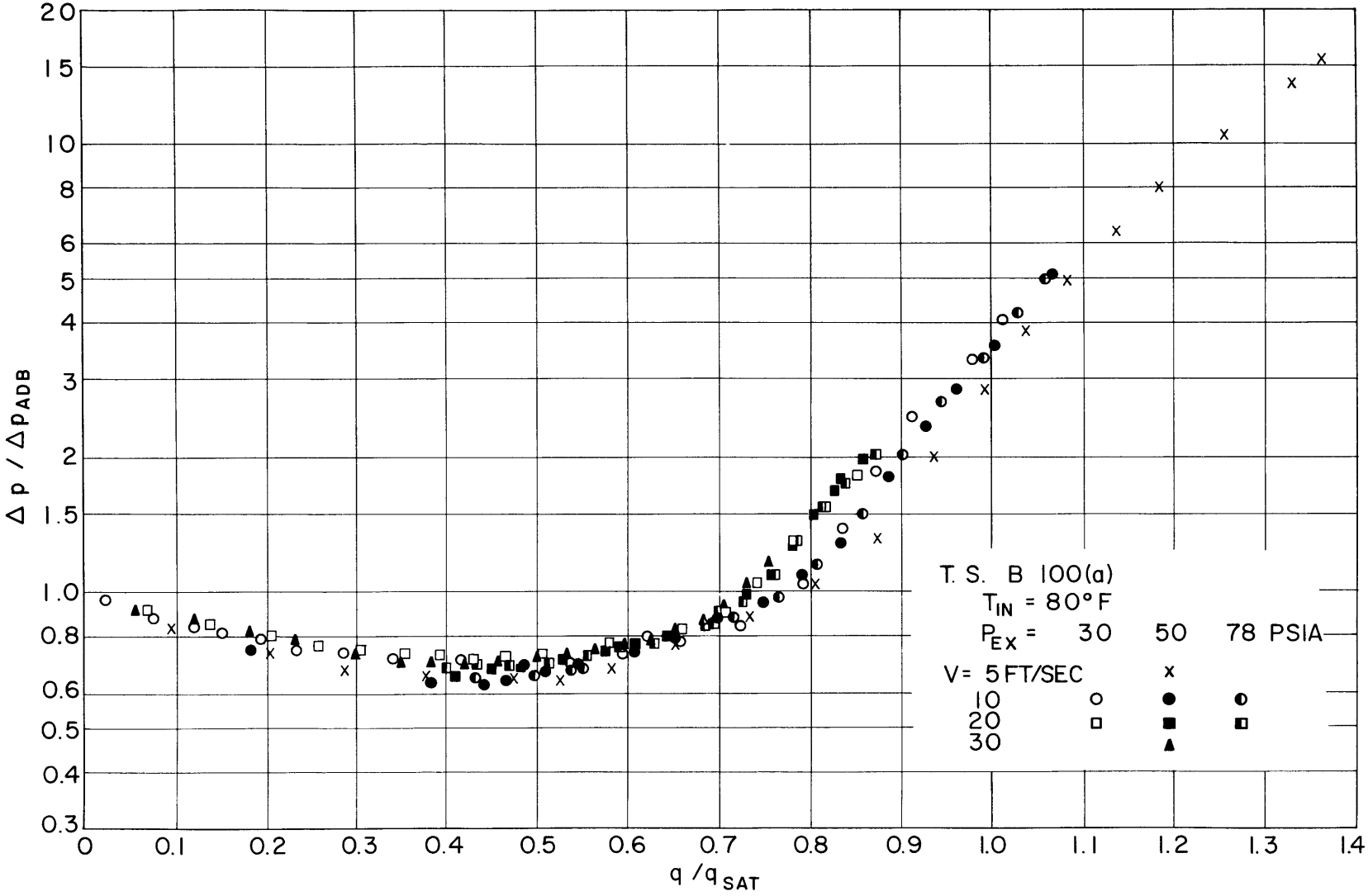

FIG. 31 CORRELATED PRESSURE DROP DATA – T. S. B 100

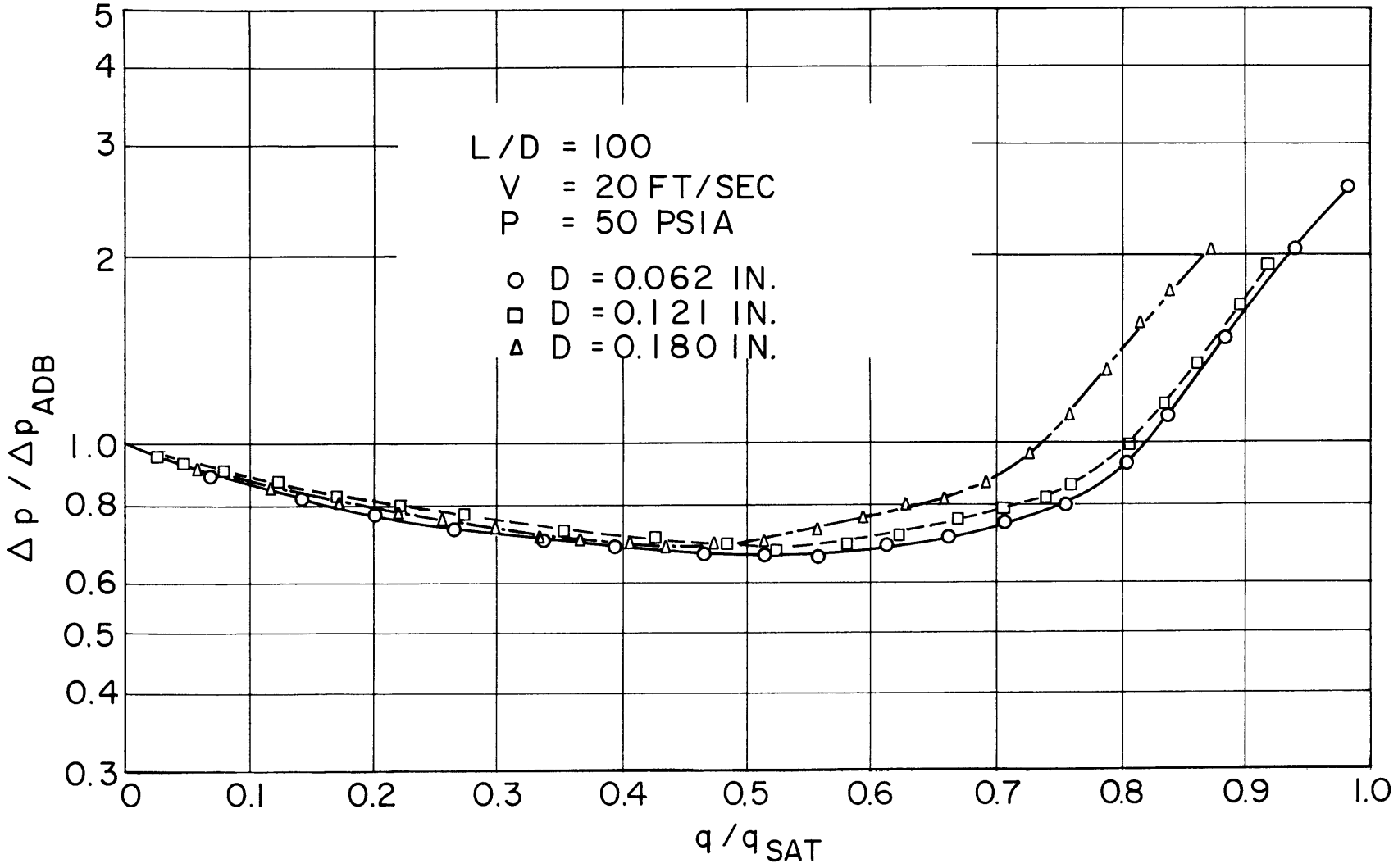

FIG. 32 CORRELATED PRESSURE DROP, DIAMETER EFFECT

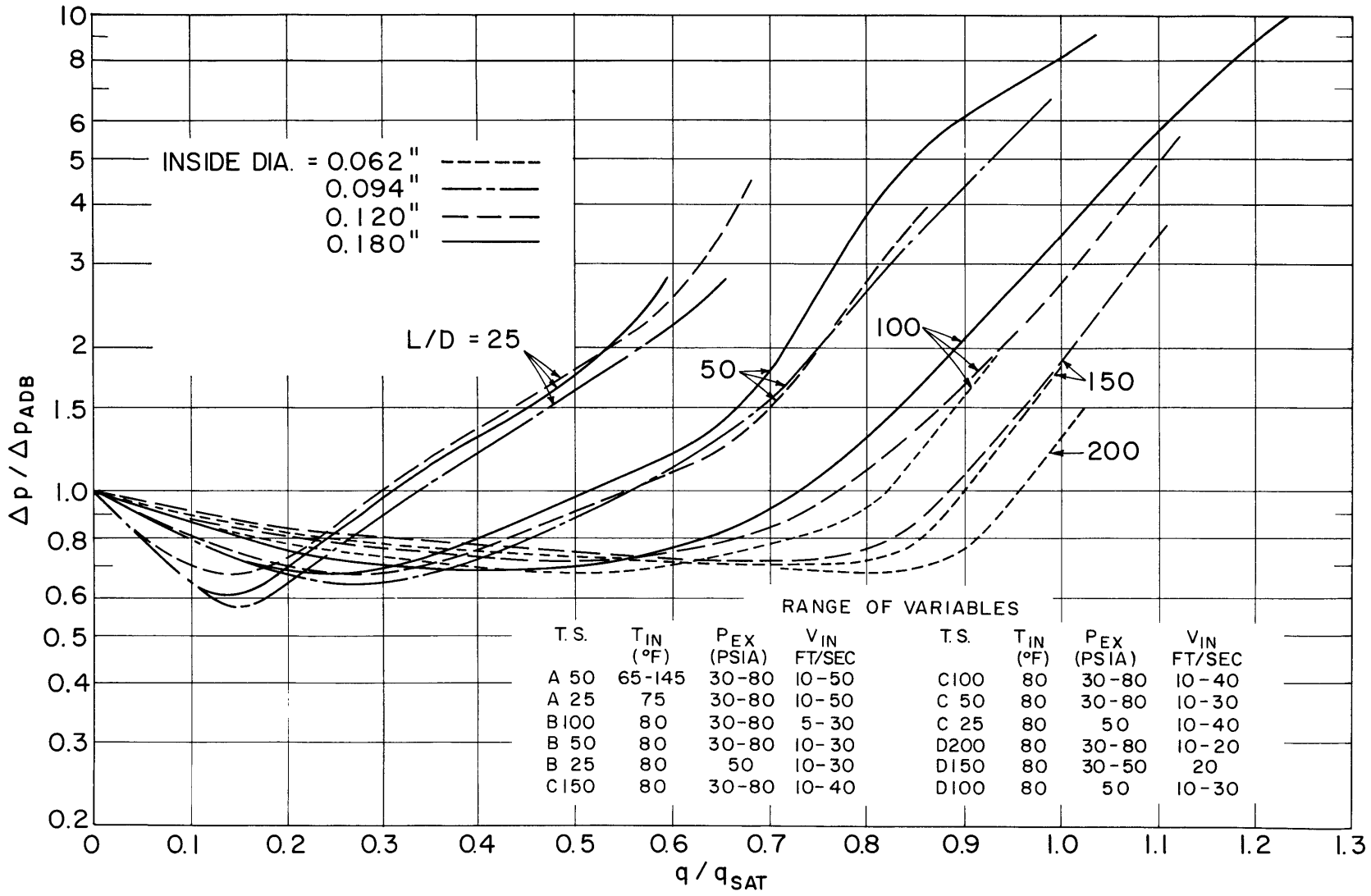

FIG. 33 CORRELATED PRESSURE DROP - ALL GEOMETRIES